Connective tissue growth factor (CCN2) is a matricellular preproprotein controlled by proteolytic activation

Received for publication, June 21, 2018, and in revised form, August 23, 2018 Published, Papers in Press, September 27, 2018, DOI 10.1074/jbc.RA118.004559

Ole Jørgen Kaasbøll[‡§], Ashish K. Gadicherla[‡§1], Jian-Hua Wang[¶], Vivi Talstad Monsen[‡§], Else Marie Valbjørn Hagelin[‡§], Meng-Qiu Dong[¶2], and Håvard Attramadal[‡§3]

From the [‡]Institute for Surgical Research, Oslo University Hospital and University of Oslo, NO-0424 Oslo, Norway, [§]Center for Heart Failure Research, University of Oslo, NO-0316 Oslo, Norway, and [¶]National Institute of Biological Sciences, 102206 Beijing, China

Edited by Alex Toker

Connective tissue growth factor (CTGF; now often referred to as CCN2) is a secreted protein predominantly expressed during development, in various pathological conditions that involve enhanced fibrogenesis and tissue fibrosis, and in several cancers and is currently an emerging target in several early-phase clinical trials. Tissues containing high CCN2 activities often display smaller degradation products of full-length CCN2 (FL-CCN2). Interpretation of these observations is complicated by the fact that a uniform protein structure that defines biologically active CCN2 has not yet been resolved. Here, using DG44 CHO cells engineered to produce and secrete FL-CCN2 and cell signaling and cell physiological activity assays, we demonstrate that FL-CCN2 is itself an inactive precursor and that a proteolytic fragment comprising domains III (thrombospondin type 1 repeat) and IV (cystine knot) appears to convey all biologically relevant activities of CCN2. In congruence with these findings, purified FL-CCN2 could be cleaved and activated following incubation with matrix metalloproteinase activities. Furthermore, the C-terminal fragment of CCN2 (domains III and IV) also formed homodimers that were ~20-fold more potent than the monomeric form in activating intracellular phosphokinase cascades. The homodimer elicited activation of fibroblast migration, stimulated assembly of focal adhesion complexes, enhanced RANKL-induced osteoclast differentiation of RAW264.7 cells, and promoted mammosphere formation of MCF-7 mammary cancer cells. In conclusion, CCN2 is synthesized and secreted as a preproprotein that is autoinhibited by its two N-terminal domains and requires proteolytic processing and homodimerization to become fully biologically active.

CCN2 is the most studied member of a family of secreted glycoproteins termed CCN proteins (acronym of Cyr61/CTGF/Nov). CCN2 is implicated in several diseases (1), in particular diseases in which enhanced fibrogenesis and tissue fibrosis are a characteristic pathophysiologic feature. In this context, CCN2 has been reported to be among the 10 most abundant transcripts in primary human fibroblasts and thus plays an important role in defining the phenotypic characteristics of the fibroblast (2, 3). Although the designation "connective tissue growth factor" (CTGF)[4] implies that CCN2 may act as a growth factor, the prevailing opinion in the field is that the actions of CCN2 are not limited to that of growth factors *per se*. The CCN proteins contain up to four structural domains that are highly conserved among the family. Following the second structural domain is a nonconserved unstructured "hinge" region of variable length that connects the third domain (a schematic of modular organization is depicted in Fig. 1*a*). Although the role of the modular structure of CCN proteins is poorly understood, this structural organization has fostered the hypothesis that CCN proteins are matricellular proteins (4–7) to refer to a group of secreted proteins with diverse regulatory roles at the interface of the extracellular matrix and the cell surface. According to this paradigm the complex regulatory actions of CCN2 are made possible by diverse protein–protein interactions involving the different domains of CCN2 (4–7). However, the categorization of CCN proteins as matricellular proteins (4–7) may have dissuaded studies on the structure-activity relationships of CCN2 as a signaling molecule. In several reports on mice genetically engineered to overexpress FL-CCN2, rather limited phenotypes have been observed in the absence of experimentally induced disease (8, 9). One interpretation of these findings could be that CCN2 must undergo further processing to become biologically active. In this respect, smaller fragments of CCN2 from 10 to 20 kDa have also been observed in some

This work was supported by the Norwegian Council for Cardiovascular Research (to O. J. K.) and Scientia fellowship program, University of Oslo (to A. K. G.). The authors declare that they have no conflicts of interest with the contents of this article.

This article contains Figs. S1–S7 and Tables S1 and S2.

[1] Present address: Max Planck Institute of Biophysics, D-60438 Frankfurt am Main, Germany.

[2] Supported by Ministry of Science and Technology of China Grant 973-2014CB84980001.

[3] Supported by a grant from the South Eastern Norway Regional Health Authority. To whom correspondence should be addressed: Oslo University Hospital, Institute for Surgical Research-A3.1057, P. O. Box 4950 Nydalen, NO-0424 Oslo, Norway. Tel.: 47-23073520; E-mail: havard.attramadal@medisin.uio.no.

[4] The abbreviations used are: CTGF, connective tissue growth factor; FL-CCN2, full-length CCN2; CHO, Chinese hamster ovary; RANKL, receptor activator of nuclear factor κB ligand; TGFβ, transforming growth factor β; EGF, epidermal growth factor; VEGF, vascular endothelial growth factor; ERK, extracellular signal–regulated kinase; S6K, p70 S6 kinase; RSK, p90 ribosomal S6 kinase; CI, confidence interval; aa, amino acids; EMT, epithelial-to-mesenchymal transition; MMP, matrix metalloproteinase; vWC, von Willebrand type C repeat; BMP, bone morphogenetic protein; DHFR, dihydrofolate reductase; SUMO, small ubiquitin-like modifier; DMEM, Dulbecco's modified Eagle's medium; PVDF, polyvinylidene difluoride; AUC, area under the curve; 4SBE, four SMAD-binding response elements; DAPI, 4′,6-diamidino-2-phenylindole; MTT, 3-(4,5-dimethylthiazol-2-yl)-2,5-diphenyltetrazolium bromide; TRAP, tartrate-resistant acid phosphatase; ANOVA, analysis of variance; SNAIL, zinc finger protein SNAI1; GAPDH, glyceraldehyde-3-phosphate dehydrogenase.

tissues that display high activities of CCN2 (10–12) (see also Fig. S1, *a* and *c*). Indeed, some of these fragments have previously been shown to display biologic activity (11, 13–17). For example, the 10-kDa C-terminal fragment of CCN2 (comprising the cystine knot domain) isolated by Brigstock and co-workers (14, 15) and produced by recombinant DNA technology is widely used and has reported capacity for eliciting cell signaling responses (18–20). However, as previously reported from our laboratory, the potency of the 10-kDa fragment in eliciting rapid cell signaling responses is very low compared with the presumptive full-length 37-kDa CCN2 (19). Interestingly, a recent report by Mokalled *et al.* (21) showed that genetic overexpression of an N-terminally truncated form of CCN2 containing only domains III and IV was sufficient and even appeared to be more effective than full-length CCN2 in mediating spinal cord regeneration in a zebrafish model of injury to the spinal cord. Thus, the time has come to assess the efficacies and potencies of full-length CCN2 and the various fragments of CCN2 that can be isolated following secretion of CCN2. In this report, we address the fundamental question of to what extent CCN2 is secreted as a preproprotein that needs to undergo proteolytic processing to become a biologically active signaling molecule. Although this issue is not an imminent research question in the field of CCN proteins, release of fragments with signaling capacity is certainly well established for many other autocrine/paracrine factors (22), structural extracellular matrix proteins (matrikines) (23), and even some matricellular proteins (24–26). Thus, the major goal of this study was to resolve the structure-activity relationships of fully active CCN2. Finally, we investigated to what extent the structure-activity relationships of bioactive CCN2 may also apply for CCN1 and CCN3.

Results

Characterization of CCN2 entities

Western blot analysis of the cell culture medium of DG44 CHO cells engineered to produce and secrete FL-CCN2 revealed several bands immunoreactive to anti-CCN2 antibodies. Based on the presumptive hypothesis that CCN2 undergoes proteolytic activation following secretion, the different entities of CCN2 were separated through several chromatographic steps and subsequently subjected to structural analysis and investigation of biologic activity. Separation of different entities of CCN2 was complicated by the dispersed isoelectric points attributed to the varying glycosylation pattern of CCN2 (27) (Fig. S1, *a* and *b*). However, the following CCN2 entities were purified to apparent homogeneity (Fig. 1 for Western blotting analyses and Fig. S2 for purification scheme and MS data) and designated as follows. 1) FL-CCN2-M is the 37-kDa full-length CCN2 monomer. 2) FL-CCN2-D is a 60-kDa entity immunoreactive to anti-CCN2 antibodies and migrating as 37-kDa in the presence of β-mercaptoethanol (confirmed by MS analysis to represent a homodimer of full-length CCN2). 3) CT-CCN2 is a band migrating at 18 kDa under reducing conditions, confirmed by Western blot analysis and MS analysis to be a C-terminal fragment of CCN2 comprising domains III (TSP1) and IV (cystine knot) with N-terminal identity ^{181}AYRLED^{186}. This C-terminal fragment of CCN2 generated by endopeptidase cleavage of the amide bond between Ala^{180} and Ala^{181} is consistent with previously reported endopeptidase cleavage fragments of CCN2 (28). 4) NT-CCN2 is the N-terminal 17-kDa fragment of CCN2. In our experience, commercially available antibodies against NT-CCN2 displayed poor avidity and specificity; hence, the identity of NT-CCN2 was determined by MS analysis to constitute domains I and II (Fig. S2*e*).

During the initial activity testing of the purified CCN2 entities, it became clear that for some of the CCN2 entities (for example the 37-kDa CCN2 entity) signaling activity was diminished or eventually lost as progressively purer CCN2 entities were obtained. Also, the concentrations of the 18-kDa CT-CCN2 fragment required to elicit CCN2 signaling responses were substantially higher than what we observed at earlier stages of the purification. Thus, we attempted to purify CCN2 entities based on specific activities (activity/μg of protein) from sequential chromatographic steps to uncover whether even less prominent CCN2 entities with higher specific activities could be present. To expedite screening of the signaling activity of the various CCN2 fractions eluted from the different chromatographic steps, we modified a FRET-based AKT kinase-activity biosensor (29) by exchanging the FRET chromophores with fragments of NanoLuc luciferase to generate a biosensor based on enzyme complementation of NanoLuc luciferase activity (30) (Fig. 2*a*), yielding an assay with substantially improved signal-to-noise ratio compared with the FRET readout (29). The resulting biosensor assay, henceforth referred to as Nano-iAKT, was stably transfected into CCN2-responsive Rat2 cells (31) and validated with AKT inhibitors (see Fig. S3 for biosensor validations). The eluted fractions of each chromatographic step were then assessed for the ability to stimulate AKT kinase activity. Fractions that stimulated AKT were subsequently subjected to Western blot analysis of CCN2 immunoreactivities using antibodies directed at various domains of CCN2. Western blot analyses of the resulting fractions were performed under both reducing and nonreducing conditions as the C-terminal cystine knot domain of CCN2 is postulated to engage in protein dimer formation (32). This strategy made it possible to separate an immunoreactive entity comigrating with the far more abundant FL-CCN2-M around 37 kDa in the absence of β-mercaptoethanol and migrating at 18 kDa in the presence of β-mercaptoethanol (F16 in Fig. S1*e*), suggesting that this entity might represent a homodimer of the 18-kDa fragment. Fractions containing the latter CCN2 entity displayed the highest specific activities among the various CCN2 entities assessed by the Nano-iAKT assay (*e.g.* fraction 16 in Fig. S1*f*).

Western blot analysis of myocardial tissue extracts subjected to electrophoresis under nonreducing conditions also revealed a band migrating at ~60 kDa that was immunoreactive to anti-CCN2 IgG (Fig. S1*c*). However, under reducing conditions, the immunoreactivity at 60 kDa disappeared, and the predominant immunoreactivity was observed around 37 kDa (Fig. S1*c*). In congruence with the fragments isolated and purified from the DG44 CHO cells expressing full-length CCN2, anti-CCN2 (C-terminal) immunoreactivity migrating at ~18 kDa appeared in extracts of granulation tissue from infarcted hearts separated

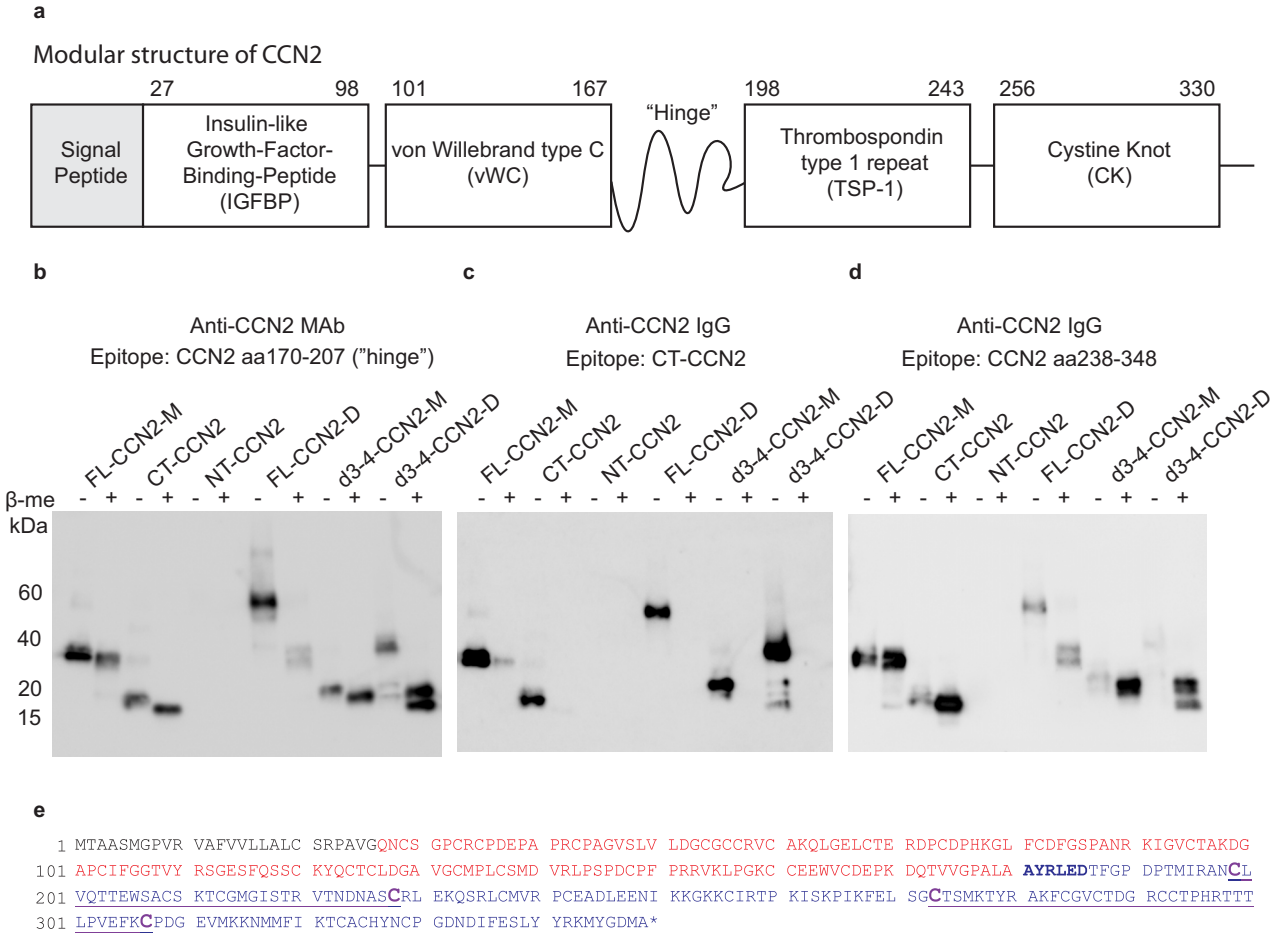

Figure 1. Characterization of purified CCN2 entities. *a*, schematic of the modular structure of CCN2. *b–d*, equal amounts (μg of protein) of purified preparations of different entities of CCN2 were incubated in the absence or presence of β-mercaptoethanol (5%, v/v) before SDS-PAGE for separation of nonreduced and reduced proteins, respectively. *b*, Western blot analysis with antibody directed against epitopes in the hinge region of CCN2 demonstrates the expected immunoreactivity with molecular mass around 37 kDa for both nonreduced and reduced FL-CCN2-M, validating the antibody's usefulness for detection of both nonreduced and reduced CCN2. The d3-4-CCN2 preparations are readily detected too, as the hinge epitopes were included in the d3-4-CCN2 construct to enable the utilization of the hinge antibody for detection of nonreduced d3-4-CCN2 protein preparations. The FL-CCN2-D preparation displays immunoreactivity that migrates at 60 kDa under nonreducing conditions and shifts to 37 kDa under reducing conditions. The d3-4-CCN2-D preparation migrates at approximately 40 kDa under nonreducing conditions, whereas immunoreactivities appear between 17 and 20 kDa under reducing conditions. Subsequently, CT-CCN2 (purified from the FL-CCN2–secreting DG44 CHO cell line) was used as immunogen to generate IgG with higher avidity toward nonreduced protein preparations containing domains III-IV of CCN2 (*c*). As shown in *c*, the anti-CT-CCN2 IgG preferentially identified nonreduced CCN2 fragments, confirming the migration patterns of FL-CCN2-D and d3-4-CCN2-D at 60 and 40 kDa, respectively. *d*, following reduction of the same preparations, an antibody recognizing epitopes in the C-terminal region of CCN2 did not display immunoreactivity against the NT-CCN2 preparation, whereas immunoreactivities of the other CCN2 preparations migrated as expected. Gels are representative of at least two different purifications of all the various CCN2 protein preparations. *e*, schematic illustrating the primary structure of the CCN2 entities purified from the FL-CCN2–producing cell line based on immunoblots and analysis of separated entities by MS (Fig. S2): *black*, signal peptide; *red*, NT-CCN2; *blue*, CT-CCN2, with *bold letters* indicating the N-terminal part of CT-CCN2 as identified by Edman sequencing. The cysteine residues highlighted in *purple* and connected with *purple underlining* show identified disulfide bridges in the d3-4-CCN2 preparations. FL-CCN2-M, full-length CCN2 monomer; CT-CCN2, C-terminal CCN2 (purified from FL-CCN2–producing cell line); NT-CCN2, N-terminal CCN2 (purified from FL-CCN2–producing cell line); FL-CCN2-D, full-length CCN2 dimer; d3-4-CCN2-M, domains III-IV CCN2 monomer (purified from domains III-IV CCN2–producing cell line); d3-4-CCN2-D, domains III-IV CCN2 dimer (purified from domains III-IV CCN2–producing cell line). *β-me*, β-mercaptoethanol.

in the presence of β-mercaptoethanol. However, it was not possible to discern immunoreactivity under nonreducing conditions that might represent a putative dimer of the 18-kDa band from the principal immunoreactivity migrating at 37 kDa (Fig. S1*c*).

However, as it was not possible to separate the potential dimer of the 18-kDa fragment in a substantially enriched form from the far more abundant full-length CCN2 as well as from the monomer of the 18-kDa fragment present in the cell culture medium of the FL-CCN2–producing cell line, we engineered another stable CHO cell line producing and secreting the recombinant C-terminal fragment of CCN2 comprising domains III-IV of CCN2 (d3-4-CCN2). Notably, this d3-4-CCN2–expressing cell line secreted both monomeric and dimeric d3-4-CCN2. Thus, from the cell culture medium of this cell line, we were able to purify (Fig. 1 and Fig. S2*b*) and characterize the monomeric (d3-4-CCN2-M) and dimeric (d3-4-CCN2-D) d3-4-CCN2 entities.

Monomeric and dimeric d3-4-CCN2 were subjected to LC-MS/MS, and the identified fragments were analyzed by pLink-SS, an algorithm for MS-based identification of disulfide bridges (33, 34). The analysis revealed that of the 16 cysteines in domains III-IV four were detected as forming disulfide bridges in both d3-4-CCN2-M and d3-4-CCN2-D, *i.e.* Cys^{199}-Cys^{228}

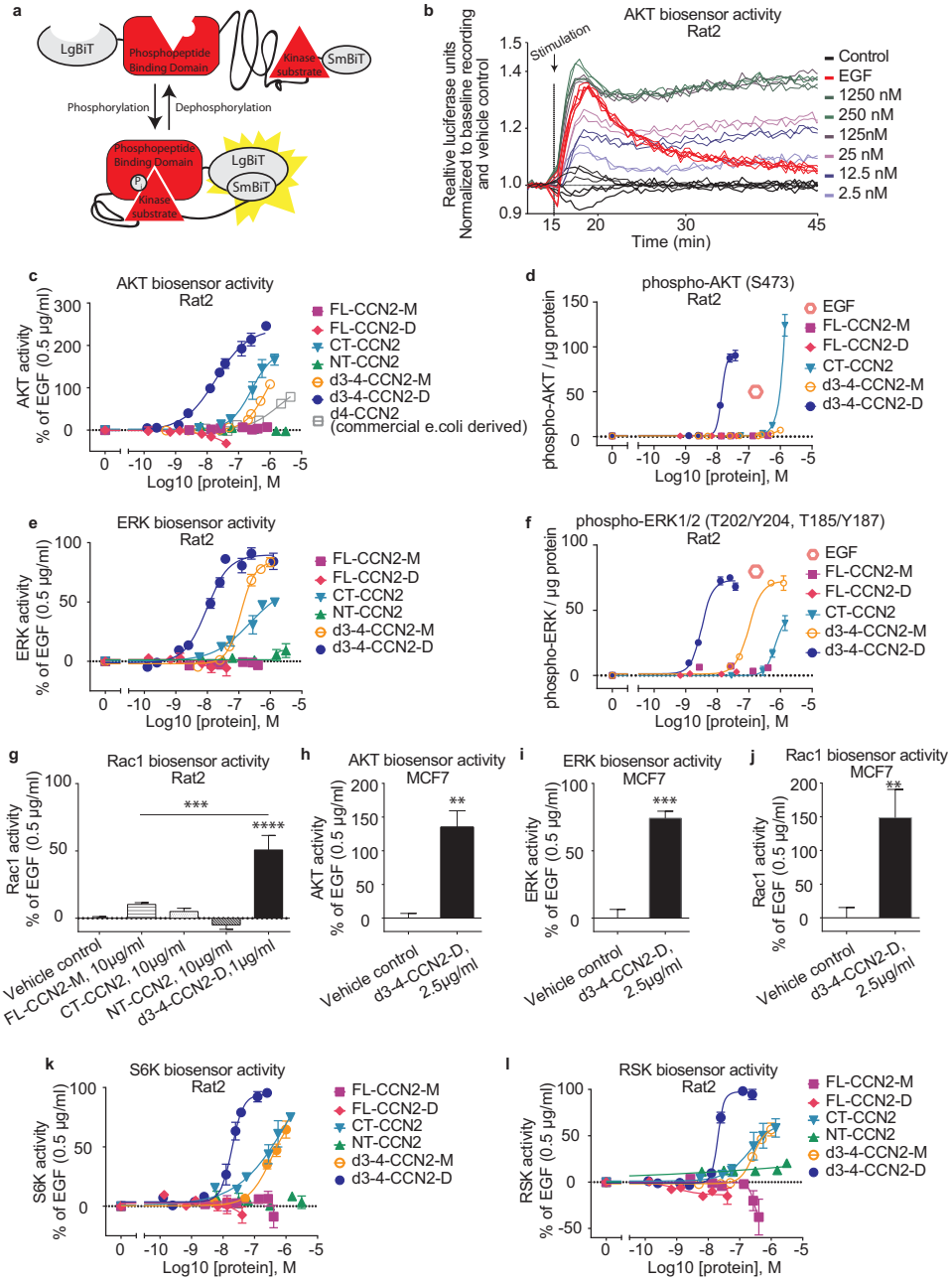

Figure 2. Signaling activities of different CCN2 entities. *a*, schematic of a biosensor of specific phosphokinase activities based on split-NanoLuc luciferase complementation (NanoBiT, Promega). Phosphorylation of the kinase substrate increases the affinity for the phosphopeptide-binding domain (forkhead-associated domain-1), resulting in alterations of the 3D structure that allow the two fragments of NanoLuc luciferase (LgBiT and SmBiT) to come in sufficient proximity to reconstitute bioluminescent luciferase activity. In the case of the biosensor for Rac1 (*g* and *j*), the kinase substrate and phosphopeptide-binding domain were substituted with Rac1 and the CRIB domain (N-terminal Cdc42/Rac interactive binding motif) from Pak1. Active GTP-bound Rac1 binds CRIB altering the 3D structure of the biosensor, allowing for complementation of NanoLuc luciferase activity as described above. *b*, real-time recordings of AKT activity upon stimulation with a range of d3-4-CCN2-D concentrations reveal instantaneous signal activation. Each *line* is data from one well, two for each concentration. *c*, *e*, and *g–l*, biosensor bioluminescence was recorded for 30 min following stimulation of serum-starved cells with the indicated CCN2 entities. AUC relative to that of the vehicle control was calculated and is presented as percentage of the positive control (0.5 μg/ml EGF). *d* and *f*, serum-starved Rat2 cells stimulated with the indicated protein preparations for 20 min were assayed with Luminex bead–based immunoassays for the indicated phosphoproteins, and signal is presented relative to total protein. $n \geq 2$ independent experiments for all assays (*c–l*). All *error bars* represent S.E. (*c–l*). All curves were generated utilizing four-variable nonlinear regression in GraphPad Prism. Statistical significance was calculated by one-way ANOVA with Šidák's post hoc test in *g* and two-tailed *t* test in *h–j*. **, $p < 0.01$; ***, $p < 0.001$; ****, $p < 0.0001$.

and Cys^{273}-Cys^{307} (Fig. S2*g*), in congruence with previous data on CCN2 from analysis of the secretome of endothelial cells (33). These disulfide bridges were most likely intraprotein bridges as they were found both in the monomeric and in the dimeric d3-4-CCN2.

As contaminating TGFβ activities in preparations of purified recombinant CCN2 have been observed,[5] we tested all the isolated CCN2 entities for activation of SMAD transcriptional

[5] L. F. Lau, personal communication.

activity using a SMAD reporter assay. In our experience, TGFβ activity (*i.e.* induction of the SMAD reporter) coeluted with CCN2 entities containing domains III-IV from ion-exchange chromatography columns, hydrophobic-interaction chromatography columns, and heparin-affinity chromatography columns. Thus, a subsequent size-exclusion chromatography step was necessary to remove contaminating TGFβ activity from the CCN2 entities. As shown in Fig. S2*c*, neither of the CCN2 preparations subjected to size-exclusion chromatography displayed detectable SMAD reporter activities except for d3-4-CCN2-M (10 μg/ml), which contained minute amounts of SMAD-stimulating activity.

Release of the C-terminal domains III-IV of CCN2 is necessary for signaling activity

Once the various CCN2 entities had been purified and characterized, we proceeded to investigate their relative potencies and efficacies in various signaling assays, starting with the Nano-iAKT biosensor assay. As demonstrated in the real-time recording shown in Fig. 2*b*, this assay allowed for detection of AKT activity within the first minutes of stimulation with d3-4-CCN2-D. Another noteworthy observation was that the time course of AKT activity following stimulation with d3-4-CCN2-D was similar to that of EGF, the positive control. However, d3-4-CCN2-D elicited more prolonged activation of AKT compared with the transient stimulation of AKT activity in the presence of EGF. As many groups have routinely used the commercially available *Escherichia coli*–derived C-terminal domain IV fragment of CCN2 (d4-CCN2), reported to confer partial CCN2 activity (15, 17), we also included this fragment of CCN2 in the Nano-iAKT assay. Only fragments containing domains III and IV or domain IV of CCN2, d4-CCN2, CT-CCN2, d3-4-CCN2-M, and particularly d3-4-CCN2-D, were able to stimulate AKT activity (Fig. 2*c*). These results confirmed our initial findings that dimer-enriched fractions of CT-CCN2, purified from the cell line producing FL-CCN2, is the most active form of CCN2. The assay also demonstrated that the CCN2 preparations containing both domains III and IV were substantially more potent and possibly also more effective than d4-CCN2. Thus, domain III appears to be required for full biological activity of CCN2. Strikingly, FL-CCN2-M and FL-CCN2-D, as well as NT-CCN2, completely lacked capacity to stimulate AKT. The concentration-effect relationships of the various CCN2 entities recorded with the AKT biosensor assay were confirmed by Luminex™ bead–based immunoassay of phospho-AKT (Ser^{473}) levels (Fig. 2*d*). As phosphorylation and activation of ERK1/2 are also a reported CCN2 activity (35, 36), we assayed the concentration-effect relationships of the different CCN2 entities both by biosensor-recorded ERK activity (Fig. 2*e*) and by determination of phospho-ERK1/2 (Thr^{202}/Tyr^{204} and Thr^{185}/Tyr^{187}) levels in Rat2 fibroblasts (Fig. 2*f*). In congruence with the assays of AKT activities, d3-4-CCN2-D was substantially more potent than d3-4-CCN2-M in stimulating ERK1/2 activities. The higher potency of d3-4-CCN2-D was also demonstrated for stimulation of Rac1 activity (Fig. 2*g*), another rapid signaling activity elicited by CCN2 (18, 37) (see Fig. S3*i* for real-time activity data). Notably, also the time course of d3-4-CCN2-D stimulated Rac1, and its sensitivity to the EGF receptor inhibitor gefitinib differed from that of EGF-stimulated Rac1 (Fig. S3, *i* and *j*). As all of the above assays were performed in Rat2 fibroblasts, we proceeded to investigate whether d3-4-CCN2 might activate the same signaling pathways in another cell line also reported to respond to CCN2. Hence, MCF-7 mammary carcinoma cells (38, 39) were stimulated with d3-4-CCN2-D, confirming that d3-4-CCN2 also stimulates AKT, ERK, and Rac1 activities in these cells (Fig. 2, *h–j*). Biosensors for p70 S6 kinase (S6K) and p90 ribosomal S6 kinase (RSK) kinase activities, *i.e.* downstream kinases previously shown to be phosphorylated in tissues overexpressing CCN2 (9), again demonstrated the same order of potencies for d3-4-CCN2-D, d3-4-CCN2-M, and CCN2-CT as those observed for stimulation of AKT and ERK activities (Fig. 2, *k* and *l*). Consistent with the assays of AKT and ERK activities, neither FL-CCN2 nor NT-CCN2 was able to stimulate S6K or RSK kinase activities (Fig. 2, *k* and *l*). Although the concentration-effect relationships of CT-CCN2– and d3-4-CCN2-M–stimulated AKT and ERK activities displayed some variations of efficacy and potency among the bioassays and immunoassays, a consistent finding was that only CCN2 entities containing domains III and IV or domain IV were capable of eliciting cell signaling activity. Furthermore, the dimeric d3-4-CCN2 (d3-4-CCN2-D) was ~20-fold more potent than the monomeric form (*e.g.* EC_{50} for d3-4-CCN2-D–stimulated ERK activities (biosensor), 9.5×10^{-9} M (95% CI, 7.4×10^{-9}–1.2×10^{-8}), *versus* EC_{50} for CT-CCN2-stimulated ERK, 2.2×10^{-7} M (95% CI, 3.9×10^{-8}–1.3×10^{-6})). Altogether, the signaling assays consistently confirmed our hypothesis that proteolytic processing of FL-CCN2 is a necessary activation step for biological activity of CCN2.

C-terminal fragments of CCN2 recapitulate the cell physiologic effects of CCN2

Next we performed cell physiological assays to investigate whether the differences of efficacy and potency among the various CCN2 entities observed in the signaling assays were also reflected in the cell physiological actions previously reported for CCN2. CCN2 has been shown to stimulate a number of complex cell physiologic actions in various cells, including cell migration, adhesion, proliferation, and differentiation (4). As these assays are of a prolonged duration that may be sufficient for substantial proteolytic processing of exogenously added CCN2 to occur, we investigated to what extent recombinant FL-CCN2 added to the cell culture medium of Rat2 fibroblasts would be subjected to proteolytic cleavage within the relevant time frame. As shown in Fig. 3*a*, FL-CCN2 incubated with Rat2 fibroblasts for 24 h underwent proteolytic cleavage and generated a C-terminal fragment of ~18 kDa that was detected with a CCN2 antibody directed toward an epitope in the hinge region (aa 170–207) of CCN2. Thus, the cell physiologic assays may not provide conclusive evidence as to what extent full-length entities of CCN2 (FL-CCN2) lack biological activity; however, they may provide important information as to what extent the CCN2 fragments found to be bioactive signaling molecules also replicate the broad spectrum of cell physiologic actions previously reported for CCN2. First, the often reported capacity of CCN2 to stimulate cell migration was investigated.

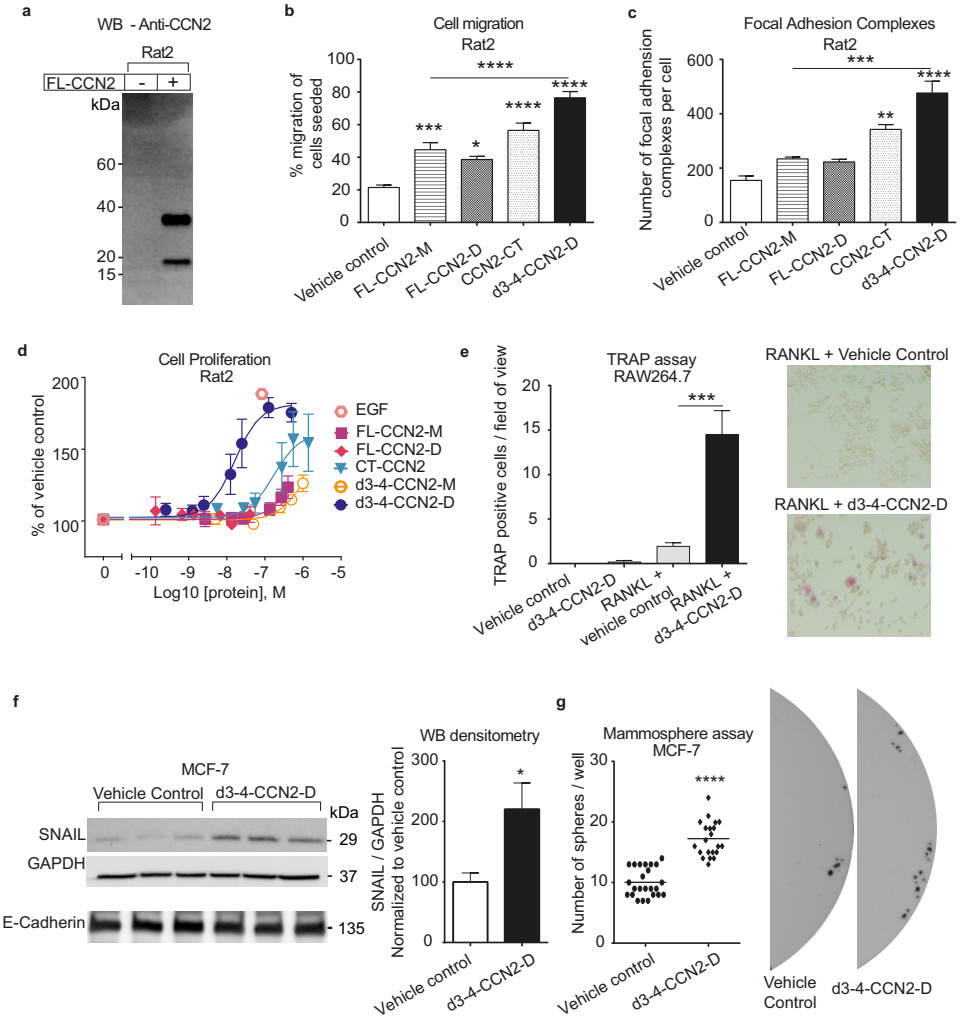

Figure 3. Cell physiological effects of different CCN2 entities. *a*, photomicrograph of Western blot (*WB*) of cell extracts from culture of Rat2 fibroblasts incubated with or without recombinant FL-CCN2-M for 24 h immunoblotted and probed with a CCN2 antibody recognizing an epitope from the hinge region (aa 170–207), demonstrating processing of FL-CCN2-M by the Rat2 cells (see Fig. 1, *b–d*, for Western blot of the same FL-CCN2-M preparation not subjected to incubation with Rat2 cells). *b*, Rat2 cells were seeded in the upper compartment of Boyden chambers and serum-starved for 16–20 h, subsequently the indicated CCN2 preparations (0.5 μg/ml) were added to the lower chamber, and incubation continued for another 16 h. Cells migrating to the underside of the chambers were stained and counted, and migration was expressed as percentage of seeded cells. *c*, Rat2 cells were serum-starved for 16–20 h and stimulated with the indicated CCN2 preparations (0.5 μg/ml) before fixation and immunostaining for vinculin and focal adhesion kinase, whereupon colabeled foci were counted as focal adhesion complexes. $n = 3$ biologically independent experiments for *b* and *c*. Representative photomicrographs are included in Figs. S4*a* and S5. *d*, Rat2 cells were serum-starved for 16–20 h, subsequently stimulated in the presence of the various CCN2 preparations for 48 h as indicated, and subjected to assay of cell proliferation using the CellTiter-Glo kit ($n = 2$ independent experiments). The data were subjected to curve fitting using four-variable nonlinear regression in GraphPad Prism. *e*, RAW264.7 cells were maintained in culture medium containing 0.5% fetal calf serum and stimulated with 1 μg/ml d3-4-CCN2-D in the presence or absence of 10 ng/ml RANKL, incubated for 7 days, and stained for TRAP. Panels to the *right* show representative photomicrographs of TRAP-stained wells ($n = 3$ independent experiments). *f*, MCF-7 cells were maintained in culture medium containing 0.5% fetal calf serum with or without 2.5 μg/ml d3-4-CCN2-D for 72 h. Cell extracts were immunoblotted for the indicated proteins ($n = 3$). Representative blots of three independent experiments are shown with a histogram of the densitometric analyses shown to the *right*. *g*, single-cell suspensions of MCF-7 cells were cultured in mammosphere-forming conditions with or without 2.5 μg/ml d3-4-CCN2-D for 7 days, stained for cell viability with the tetrazolium dye MTT, and semiautomatically quantified. Data points are replicates from three independent experiments. Representative photomicrographs are shown in the *right panel*. Statistical significance was calculated by one-way ANOVA with Šidák's post hoc test in *b*, *c*, and *e* and two-tailed *t* test in *f* and *g*. *, $p < 0.05$; **, $p < 0.01$; ***, $p < 0.001$; ****, $p < 0.0001$. All *error bars* represent S.E. (*b–g*). Uncropped immunoblots are shown in Fig. S7. *GAPDH*, glyceraldehyde-3-phosphate dehydrogenase.

In congruence with previous reports (for a review, see Rachfal and Brigstock (4)), we found that FL-CCN2 to some degree stimulated cell migration of Rat2 fibroblasts. However, CCN2-CT and, to an even greater extent, d3-4-CCN2-D displayed substantially higher efficacy than the full-length CCN2 variants (FL-CCN2-M and FL-CCN2-D) in stimulating cell migration (Fig. 3*b* and Fig. S4*a*). We subsequently proceeded to investigate the capacity of CCN2 to increase assembly of focal adhesion complexes (37), a critical step in cell adhesion (40). Again, consistent with the signaling assays, d3-4-CCN2-D was the more effective CCN2 entity in stimulating assembly of focal adhesion complexes. However, neither of the full-length CCN2 entities elicited a significant increase of focal adhesion complexes (Fig. 3*c* and Fig. S5).

As CCN2 has been reported to stimulate either cell proliferation (31) or senescence (41) depending on cell type, Rat2 cells, an immortalized fibroblast cell line that has previously been shown to respond with cell proliferation upon stimulation with CCN2, was used (31). Thus, in subsequent experiments, we investigated the capacity of the various CCN2 entities to stim-

ulate proliferation of Rat2 fibroblasts. As shown by the concentration-effect curves in Fig. 3*d*, d3-4-CCN2-D displayed remarkably higher potency and efficacy than any of the other CCN2 entities in stimulating cell proliferation. On the contrary, the full-length CCN2 entities FL-CCN2-M and FL-CCN2-D displayed no or minimal activity below 270 nM (10 μg/ml FL-CCN2-M), consistent with the cell signaling assays. The higher potency of d3-4-CCN2-D was also reflected in DNA synthesis assayed by incorporation of bromodeoxyuridine (BrdU) (Fig. S4, *b* and *c*), validating the observation that proteolytic processing of CCN2 and generation of a homodimer of domains III and IV are required for CCN2 to exert its full mitogenic potential.

In subsequent experiments, we investigated to what extent d3-4-CCN2-D could also evoke the reported CCN2-induced osteoclast differentiation (42) and epithelial-to-mesenchymal transition (EMT) (43). Once more, d3-4-CCN2-D recapitulated the previously reported effects of CCN2, first by inducing osteoclast differentiation of RAW264.7 cells (Fig. 3*e*) and next by inducing the EMT transcription factor SNAIL and stimulating the formation of mammospheres in cultures of MCF-7 cells (Fig. 3, *f* and *g*). As the increased levels of SNAIL were not accompanied by a concomitant decrease in E-cadherin, the induction of SNAIL by d3-4-CCN2-D in these experiments most likely reflected partial EMT or induction of EMT in a small proportion of cells only.

Proteolytic cleavage of the CCN2 hinge releases the C-terminal fragment and is sufficient for activation

Having firmly established that the homodimer of the C-terminal fragment of CCN2 consisting of domains III and IV is the fully active CCN2 signaling molecule, we turned our focus to the proteolytic processing and activation of FL-CCN2. Although several proteases potentially could cleave CCN2 (28, 44–49), we chose to focus on the matrix metalloproteinases (MMPs), which have previously been shown to cleave CCN2 in the unstructured hinge region between domains II and III (28, 47–49). Incubation of FL-CCN2 with recombinant catalytic domains of various MMP isoforms revealed that FL-CCN2 was indeed susceptible to cleavage by all of the investigated MMPs except MMP11 as shown in the Western blot in Fig. 4*a*. Thus, we subsequently investigated to what extent the presence of batimastat, a broad spectrum MMP inhibitor, in the cell culture medium of the CHO cell line producing FL-CCN2 could inhibit endopeptidase cleavage of secreted FL-CCN2 and consequently reduce the generation of smaller fragments of CCN2. As shown in Fig. 4*b*, inhibition of MMPs did decrease proteolytic fragmentation of secreted FL-CCN2, indicating that MMPs were at least partially responsible for the processing of FL-CCN2 secreted from the CHO cell line. Furthermore, the recombinant MMPs that cleaved FL-CCN2 all generated similar immunoreactive fragments migrating between 15 and 20 kDa as shown in the Western blot probed with an anti-CCN2 antibody recognizing epitopes in the hinge region of CCN2 (Fig. 4*a*). This cleavage pattern was highly suggestive of the MMPs cleaving FL-CCN2 close to the cleavage site in the hinge region, generating the biologically active CT-CCN2 fragment isolated from the FL-CCN2–producing CHO cell line. The cleavage site of the latter was mapped by Edman sequencing to be the amide bond between Ala^{180} and Ala^{181} in the hinge region of CCN2 (Fig. 1*e* and Fig. S2*f*). This site has previously been reported to be a major MMP site in the hinge region of CCN2 (47, 48). Thus, to investigate to what extent the MMPs found to cleave purified recombinant FL-CCN2 could cleave at the activation site mapped for CT-CCN2, we generated a protease biosensor that contained a short peptide fragment flanking this site in the hinge of CCN2, ^{177}PALAAYRLE^{185} (Fig. 4*c*). Incubation of the biosensor with recombinant catalytic domains of various MMPs demonstrated that MMP-7, -8, -12, and -13 cleaved the ^{177}PALAAYRLE^{185} peptide sequence (Fig. 4*d*) and thus potentially represent proteases that may generate bioactive CCN2. To address the latter issue, we investigated to what extent any of the above MMP isoforms would generate bioactive CCN2 upon cleavage of FL-CCN2. Recombinant MMP8 was chosen for this purpose for the following reasons. MMP8 could be completely inhibited by batimastat (Fig. 4*a*), it could cleave CCN2 within the ^{177}PALAAYRLE^{185} region and thus generate a C-terminal fragment of CCN2 similar to the bioactive CT-CCN2 (Fig. 4*d*), and it did not display protease activity that interfered with the Nano-iAKT biosensor *per se*. As shown in Fig. 4*e*, incubation of FL-CCN2-M with MMP8 conferred a robust gain of AKT kinase activity that was sensitive to batimastat, providing proof of principle that cleavage of FL-CCN2 is both necessary and sufficient for generation of bioactive CCN2 as schematically illustrated in Fig. 4*f*.

Generation of a dimeric d3-4-CCN2 fusion protein with full agonist activity

To enable simplified production and purification of dimeric d3-4-CCN2, the fully active form of CCN2, we created fusion proteins of domains III and IV of CCN2 (d3-4-CCN2) and an Fcγ receptor–silenced version of the Fc fragment of IgG4 (50, 51). Several fusion proteins were engineered with different orientations of d3-4-CCN2 relative to the Fc fragments and varying linkers between the two entities as steric factors are known to be crucial for the efficacy and potency of Fc fusion proteins (51–53). This strategy utilized the disulfide-linked dimerization of the Fc fragment to dictate dimerization of the fusion protein. Different orientations of the Fc fragment relative to d3-4-CCN2, as well as different linkers providing varying degrees of flexibility, generated fusion proteins with various potencies and efficacies in stimulating AKT and ERK activities (Fig. 5, *a*–*c*). As shown in Fig. 5, *b* and *c*, the fusion protein in which a short linker is connecting IgG4 Fc to the C-terminal end of d3-4-CCN2 displayed agonist properties with efficacy and potency similar to those of homodimeric d3-4-CCN2-D in stimulating AKT and ERK activities, *e.g.* EC_{50} for d3-4-CCN2-D–stimulated ERK activities (biosensor), 9.5×10^{-9} M (95% CI, 7.4×10^{-9}–1.2×10^{-8}), and for d3-4-CCN2–SL–Fc, 1.3×10^{-8} M (95% CI, 1.1×10^{-8}–1.4×10^{-8}). These findings verified the importance of the homodimeric structure for maximal potency of the CCN2 fragment containing domains III-IV of CCN2.

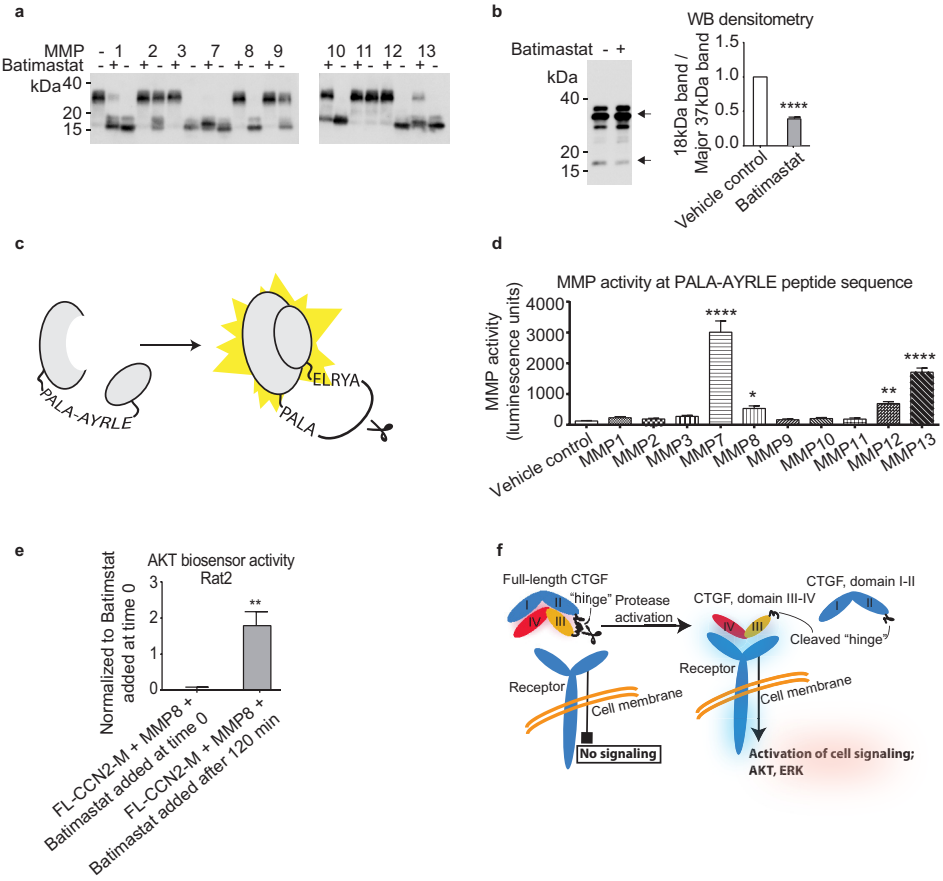

Figure 4. MMP-catalyzed cleavage and activation of CCN2. *a*, FL-CCN2-M (1 μg of protein) was incubated for 2 h with 0. 1 μg of the indicated MMPs in the presence or absence of the broad spectrum MMP inhibitor batimastat (1 μM) and immunoblotted against CCN2 (epitope aa 238–348). A representative blot of two independent experiments is shown. *b*, FL-CCN2–producing CHO cells were maintained with or without batimastat (1 μM) for 4 days, and conditioned medium was subsequently subjected to Western blot (*WB*) analysis of CCN2 immunoreactivity (epitope aa 170–207). The panel shows a representative Western blot and histogram of densitometric analysis plotted as density of immunoreactivity migrating at 18 kDa relative to the density of the immunoreactive band around 37 kDa presented as mean ± S.E. ($n = 3$). *c*, schematic of a firefly luciferase–based protease biosensor. Upon cleavage of the inserted ^{177}PALAAYRLE^{185} peptide fragment of the CCN2 hinge, the structural constraints on complementation of activity by the C-terminal and N-terminal parts of firefly luciferase are relieved, and luciferase activity is generated. *d*, the ^{177}PALAAYRLE^{185} protease sensor was stably expressed with a signal peptide directing secretion from CHO cells (CHO FreeStyle). Conditioned medium from this CHO cell line was incubated with various MMPs (2.5 ng/μl) as indicated, and luciferase activity was recorded continuously ($n = 4$ independent experiments). *e*, FL-CCN2-M was incubated with MMP8 for 120 min, and batimastat was added either from the start of incubation or at the end of the incubation period. The cleavage reactions were subsequently added to the cell culture wells of Rat2 cells stably transfected with the AKT-activity biosensor, and AKT activities were recorded ($n = 3$ independent experiments). The amount of CCN2 in each well corresponded to 24 μg/ml FL-CCN2-M. *f*, schematic model of CTGF activation (depicted as monomeric for simplicity). Full-length CTGF requires activation by proteolytic cleavage of the hinge region to release the biologically active C-terminal fragment comprising domains III and IV. Statistical significance was calculated by one-way ANOVA with Dunnett's post hoc test in *d* and two-tailed *t* test in *b* and *e*. *, $p < 0.05$; **, $p < 0.01$; ****, $p < 0.0001$. All *error bars* represent S.E. (*b*, *d*, and *e*). Uncropped immunoblots are shown in Fig. S7.

C-terminal domains (III-IV) of CCN1 and CCN3 elicit cell signaling activity

Having delineated the structure-activity relationships of CCN2, we subsequently investigated to what extent domains III and IV of other CCN family proteins would also be sufficient for activity and to what extent cleavage of the full-length proteins would be required for agonist activity. CHO cells were genetically engineered to secrete full-length CCN1 (also known as Cyr61) or CCN3 (also known as Nov) as well as the respective C-terminal fragments of CCN1 and CCN3 (containing domains III and IV). The recombinant proteins were subsequently purified from the cell culture medium. As opposed to full-length CCN2, full-length CCN1 displayed significant agonist efficacy as assessed by rapid stimulation of AKT and ERK activities in Rat2 cells (Fig. 5, *f* and *g*). However, in congruence with the structure-activity properties of CCN2, the C-terminal fragment of CCN1 containing domains III and IV displayed somewhat higher efficacy and potency than those of full-length CCN1 in stimulating AKT and particularly ERK activities, indicating that proteolytic activation may also be important in regulation of CCN1 activities (Fig. 5, *f* and *g*). Indeed, monomeric d3-4-CCN1 displayed similar potency and efficacy as monomeric d3-4-CCN2 in stimulating AKT and ERK activities (*e.g.* EC_{50} for d3-4-CCN2-M–stimulated ERK activities (biosensor), 1.2×10^{-7} M (95% CI, 9.3×10^{-8}–1.4×10^{-7}), and for d3-4-CCN1-M, 2.5×10^{-8} M (95% CI, 2.0×10^{-8}–3.2×10^{-8})). Furthermore, the migration of an immunoreactive band sensitive to β-mercaptoethanol suggested that a putative dimer of d3-4-CCN1 might exist; however, the amounts were too small to enable purification of this entity (Fig. 5*e*).

Full-length CCN3 was rapidly cleaved following secretion from the CHO cells. Thus, it was not possible to purify full-

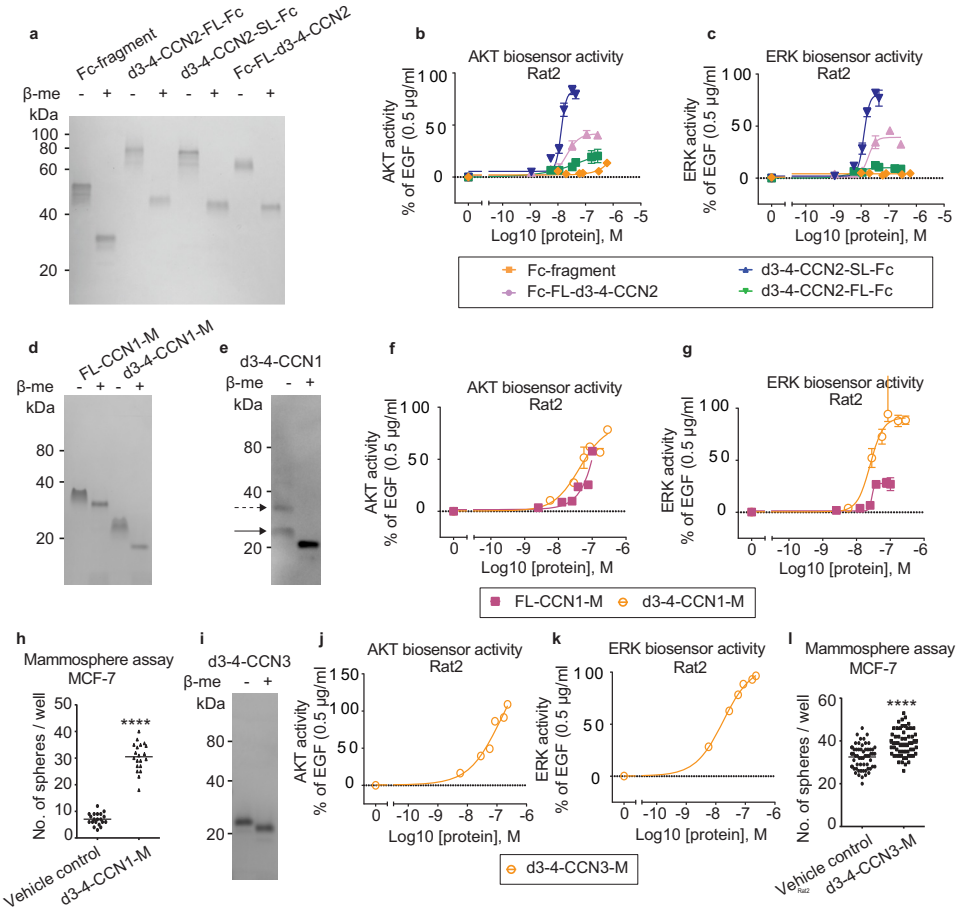

Figure 5. Signaling activities of CCN2 domains III-IV–Fc fusion proteins, CCN1 full length and domains III-IV, and CCN3 domains III-IV. *a*, Coomassie staining of nonreduced and reduced CCN2 domains III-IV–Fc fusion proteins separated by SDS-PAGE. Fc fragment, Fc fragment of IgG4 only; d3-4-CCN2–FL–Fc, domains III-IV of CCN2, a flexible linker, and Fc fragment of IgG4; d3-4-CCN2–SL–Fc; domains III-IV of CCN2, a short linker, and Fc fragment of IgG4; Fc–FL– d3-4-CCN2, Fc fragment of IgG4, a flexible linker, and domains III-IV of CCN2. *b*, *c*, *f*, *g*, *j*, and *k*, concentration-effect curves of indicated protein-stimulated AKT and ERK activities in serum-starved Rat2 cells stably transfected with the respective biosensors (see Fig. 2 for schematic) ($n = 2$ independent experiments). *d* and *i*, Coomassie staining of SDS-PAGE–separated protein preparations of FL-CCN1-M (full-length CCN1 monomer), d3-4-CCN1-M (CCN1 domains III-IV monomer), and d3-4-CCN3-M (CCN3 domains III-IV monomer). *e*, Western blot of nonreduced and reduced protein samples from the first chromatographic purification step of d3-4-CCN1 from the conditioned medium of d3-4-CCN1–producing CHO cells, demonstrating a β-mercaptoethanol–sensitive band of ~36 kDa (*dashed arrow*), twice the expected size of reduced d3-4-CCN1 (*arrow*). The blot is representative of findings from two separate purifications. *h* and *l*, single-cell suspensions of MCF-7 cells were cultured in mammosphere-forming conditions for 10 days with or without 1 μg/ml d3-4-CCN1-M or d3-4-CCN3-M as indicated, stained for cell viability with the tetrazolium dye MTT, and semiautomatically quantified. Data points are replicates from two independent experiments. All *error bars* represent S.E. (*b*, *c*, *f*–*h*, and *j*–*l*). Statistical significance was calculated by two-tailed *t* test in *h* and *l*. ****, $p < 0.0001$. *β-me*, β-mercaptoethanol.

length CCN3 from the cell culture medium of CCN3-transfected CHO cells. However, d3-4-CCN3 displayed similar efficacy and potency as d3-4-CCN1 in stimulating AKT and ERK kinase activities as shown in Fig. 5, *i*–*k* (*e.g.* EC_{50} for d3-4-CCN1-M–stimulated ERK activities (biosensor), 2.5×10^{-8} M (95% CI, 2.0×10^{-8}–3.2×10^{-8}) and for d3-4-CCN3-M, 1.8×10^{-8} M (95% CI, 1.5×10^{-8}–2.2×10^{-8}). Thus, d3-4-CCN3 is also sufficient for agonist activity of CCN3.

Subsequently, we investigated to what extent the recombinant C-terminal fragments of CCN1 (d3-4-CCN1) and CCN3 (d3-4-CCN3) were able to stimulate mammosphere formation of MCF-7 mammary carcinoma cells, a more complex biologic function. As shown in Fig. 5, *h* and *l*, both d3-4-CCN1-M and d3-4-CCN3-M stimulated mammosphere formation of MCF-7 cells, although d3-4-CCN1-M appeared to be substantially more effective than d3-4-CCN3-M.

Discussion

Still more than three decades after the discovery of CCN2 (54), a uniform protein structure that defines biologically active CCN2 has not been resolved until now. This report uncovers the novel finding that matricellular CCN2 is synthesized and secreted as a preproprotein that requires proteolytic processing to attain the capacity to elicit cell signaling responses. Furthermore, a homodimer of the active fragment, *i.e.* the C-terminal fragment comprising domains III and IV of CCN2, was shown to constitute biologically fully active CCN2. Forced generation of a homodimer of the active CCN2 fragment could be obtained by recombinant engineering of the active CCN2 fragment as fusion proteins with the Fc fragment of immunologically defective IgG4. One of these fusion proteins displayed similar efficacy and potency as the dimeric C-terminal fragment of CCN2. This new knowledge on how CCN2 acts as an autocrine/para-

crine factor may open new avenues of research on the role of CCN2 in disease mechanisms.

The finding that CCN2 is synthesized and secreted as a preproprotein that is autoinhibited by its two N-terminal domains and requires proteolytic processing and homodimerization to become fully biologically active is a mechanism shared by several other autocrine/paracrine factors, *e.g.* the TGFβ superfamily. This mechanism allows the activity of CCN2 to be controlled by an additional checkpoint, *i.e.* by specific proteases active under distinct developmental stages or under specific disease mechanisms. Interestingly, in this respect, Overall and co-workers (48) recently reported that cleavage of the hinge region of CCN family members by MMPs was more pervasive than previously appreciated.

Even though the C-terminal cystine knot domain of CCN proteins was postulated to engage in dimer formation 25 years ago (32), this is the first report on the unequivocal existence and isolation of a dimer of a CCN protein. Notably, we provide evidence that a homodimer of full-length CCN2 is not only generated in recombinant cell lines expressing full-length CCN2 but also exists *in vivo* in a tissue known to express low levels of CCN2 under physiologic conditions, *i.e.* myocardial tissue. Interestingly, in congruence with our data that CCN2 undergoes proteolytic activation, the domain III-IV fragment of CCN2 could also be demonstrated in the granulation tissue and differentiating scar tissue forming after ischemic necrosis of myocardial tissue, a process in which CCN2 is particularly involved. According to these findings, prepro-CCN2 may first form a homodimer of full-length CCN2 from which the mature homodimeric domain III-IV fragment of CCN2 is generated by proteolytic cleavage. However, we were not able to determine the levels of the homodimeric domain III-IV fragment of CCN2 in myocardial tissue as we currently do not have the means to quantitatively separate the dimeric form of domains III-IV of CCN2 from both the monomeric form of domains III-IV of CCN2 and monomeric full-length CCN2 in tissue extracts. Another hurdle is that the anti-CCN2 antibodies have different avidities toward nonreduced *versus* reduced forms of CCN2, thus making quantitative analysis of CCN2 fragments even more uncertain.

Although we did not identify any interprotein disulfide bridges responsible for homodimerization of CCN2, the pLink-SS software is limited in that not all disulfide-containing peptides may be identified, especially complex peptides containing both intraprotein and interprotein bridges (33, 34). Thus, it is still possible that any of the remaining cysteines of domains III and IV of CCN2 not demonstrated to be involved in disulfide bridge formation may engage in interprotein disulfide bridges and homodimerization of CCN2. Furthermore, another mechanism of homodimerization of CCN2 may be noncovalent metallocysteine bridge formation as demonstrated for human growth hormone (55).

In addition to conferring autoinhibition of prepro-CCN2, an important function of the N-terminal prodomains may well be to help stabilize domains III and IV of CCN2 in a conformation that would promote dimerization and secretion. Such a stabilizing function of the N-terminal prodomains would be analogous to that reported from resolution of the structure of pro-activin A (56) and from early studies that showed that expression, dimerization, and secretion of activin A and TGFβ required the presence of their prodomains (57). However, the d3-4-CCN2 fragment was undoubtedly able to dimerize and to be secreted in the absence of the N-terminal prodomains because the homodimer of d3-4-CCN2 was readily detectable in the cell culture medium from CHO cells synthesizing and secreting the d3-4-CCN2 fragment. How the prodomain affects the efficacy of dimerization and secretion of endogenously expressed full-length CCN2 remains to be resolved.

The N-terminal propeptide may also contribute to compartmentation and localization of CCN2 close to membrane-bound proteases (46, 49), facilitating activation by proteolytic cleavage of the hinge and release of the active C-terminal fragment. In this regard, it is interesting to note that domain II of CCN1 (the von Willebrand type C repeat (vWC) homology domain) has been shown to interact with transmembrane integrin $\alpha_v\beta_3$ (58), an integrin complex that has also been shown to be important for CCN2 functions (59). Also supporting a critical function of the N-terminal domains in regulation of CCN2 activities are the reports of a monoclonal anti-CCN2 antibody targeting domain II (FG-3019) for inhibition of CCN2 actions in animal disease models of pancreatic ductal adenocarcinoma (10), muscle dystrophy (60), and radiation-induced pulmonary fibrosis (61) and in early-phase clinical trials in patients suffering from idiopathic pulmonary fibrosis (62).

Domain II (vWC domain) of CCN2 has also been shown to bind other proteins in the extracellular matrix, *i.e.* proteoglycans (aggrecan) (63) and BMP-2 and -4 (64). With regard to the latter, based on X-ray crystallographic studies of the vWC domains of proteins thought to bind BMP-2, such as CV-2, collagen IIa, and CCN3, binding of the vWC domain of CCN proteins and BMP-2 has recently been questioned (65). Other domains of CCN2 may also bind proteins in the extracellular matrix. For example, domain III of CCN2 (TSP1) has been shown to bind and modulate the function of $VEGF_{165}$ (28, 47). Interestingly, MMP-mediated cleavage of CCN2 released $VEGF_{165}$ from the complex with CCN2 and caused reactivation of the angiogenic activity of $VEGF_{165}$ (28, 47). In the context of our current report, a tantalizing consequence of MMP-mediated disruption of the CCN2–$VEGF_{165}$ complex would be concerted activation of both CCN2 and $VEGF_{165}$.

Despite extensive investigations, we were not able to demonstrate any cell signaling activity responses stimulated by the N-terminal domains I and II– containing fragment of CCN2. However, in early studies, Grotendorst and Duncan (66) reported that the N-terminal fragment of CCN2 stimulated myofibroblast differentiation and collagen synthesis in the presence of insulin-like growth factor, whereas the corresponding C-terminal fragment could not. These findings were later questioned in studies by Heng *et al.* (13) and Yang *et al.* (67), which concluded that the C-terminal fragments of CCN2 could stimulate myofibroblast differentiation and collagen synthesis. Thus, these findings await further clarification.

In this report, we demonstrate that the major cleavage site in the hinge region of CCN2 generating mature CT-CCN2 was $Ala^{180} \downarrow Ala^{181}$. Interestingly, this site has also been shown to be susceptible to cleavage by ADAM28 (a disintegrin and met-

alloproteinase family endopeptidase), thus providing another example of a protease with the potential capacity to activate CCN2 (47). MMP sites in the hinge region of CCN2 have also been identified distal to the $Ala^{180} \downarrow Ala^{181}$ cleavage site (48). To what extent cleavages of CCN2 at these sites all generate a fully active CCN2 agonist may have to be investigated for each specific fragment. However, the d3-4-CCN2–Fc fusion protein in which the C-terminal fragment of CCN2 was made to commence at Ala^{197} displayed full agonist activity similar to d3-4-CCN2-D. As shown in this study, Cys^{199} forms a disulfide bridge with Cys^{228}. Thus, cleavage of CCN2 distal to Cys^{199} may perturb tertiary structure imposed by the disulfide bridge, conceivably reducing or abolishing the agonist activity of CCN2. In this respect, the 10-kDa C-terminal fragment of CCN2 comprising domain IV only, isolated by Brigstock and co-workers (14, 15), was shown to be capable of eliciting rapid cell signaling activity (18–20), although with greatly reduced efficacy and potency compared with the C-terminal fragments comprising both domains III and IV as demonstrated in this study.

For studies of cell biologic and physiologic functions, a fully active version of CCN2 that does not require prior activation would be a great advantage. Even from the dedicated d3-4-CCN2–producing cell line, the majority of the generated product was monomeric d3-4-CCN2. In contrast, the d3-4-CCN2–Fc fusion protein, which displayed agonist potency and efficacy similar to that of homodimeric d3-4-CCN2, alleviated this problem as Fc fusion proteins effectively form homodimers and provide opportunities for simple, quantitative affinity purification of the fusion protein. Furthermore, the d3-4-CCN2 fusion protein lacking immune effector function may also be attractive for investigation of *in vivo* functions of CCN2 as the Fc fragment confers prolonged half-life in the circulation (68). Biologically active Fc fusion proteins have also been reported for full-length CCN1 and CCN6 (69, 70). Although the designs of the fusion proteins in these reports were not optimized for activity, they demonstrate the potential for the application of a similar strategy for efficient production and purification of other bioactive CCN proteins as well.

An imminent question was to what extent other members of the CCN family are secreted as preproproteins that require proteolytic processing to generate the mature biologically active signaling molecules. As shown in this study, the C-terminal fragments of CCN1 and CCN3 comprising domains III and IV were clearly sufficient for activation of rapid cell signaling as well as for eliciting cell physiologic responses. Interestingly, the N-terminal domains of CCN1 also appeared to confer some degree of autoinhibition of full-length CCN1. However, full-length CCN1 did not display the strict lack of signaling activity as demonstrated for CCN2 and consequently may not be considered a preproprotein. Relative to CCN2, CCN1 has a very elongated hinge region (63 aa for CCN1 *versus* 30 aa for CCN2). Thus, the long hinge region of CCN1 could provide greater steric flexibility of the C-terminal domains III and IV, obviating the need for proteolytic cleavage to release the bioactive fragment. The pronounced susceptibility of CCN3 to endopeptidase cleavage, hampering production and purification of recombinant full-length CCN3, is consistent with previous reports (71, 72). Thus, we were not able to obtain full-length CCN3 sufficient for analysis of its agonist activity. However, indirect evidence from genetically engineered mice suggests that CCN3 may also be secreted as a preproprotein. First, mice with genetically targeted deletion of domain II (vWC) of CCN3 produce a truncated variant of CCN3 that immunologically appears to correspond to domains III and IV and displays a markedly different phenotype than both WT mice (73) and mice with complete deletion of CCN3 (74, 75). Furthermore, an N-terminally truncated variant of CCN3 has also been reported to confer transforming activity and support anchorage-independent growth of fibroblasts *in vitro*, whereas full-length CCN3 was without effect (76). These observations could be explained by proteolytic processing being necessary for activation of full-length CCN3. In this respect it is also interesting to note that the hinge region of CCN3 is very short, *i.e.* of similar length as that of CCN2. Future studies will be needed to further decipher functional differences between the CCN proteins due to differences in their hinge regions, for instance by generation of recombinant chimeras of a CCN protein and hinge regions from different CCN isoforms.

The implications of CCN2 requiring proteolytic activation to initiate signaling are very important for the interpretation of the many reports on the functions of CCN2 *in vivo* that have been published over the years. For instance, in the recently reported mice with conditional overexpression of full-length CCN2 in the kidney, no phenotype was present in the absence of a concomitant insult, whereas in the setting of ureteral obstruction, fibrosis was enhanced (20). This observation fits perfectly with the notion that in healthy adult kidney overexpression of full-length CCN2 engenders a limited phenotype, whereas in the presence of insults and concomitant release of endopeptidase activities, the effects of CCN2 overexpression become fully apparent.

Our novel finding that CCN2 is secreted as an inactive preproprotein implies that interaction with a receptor eliciting the observed cell signaling responses is not possible prior to proteolytic activation. A mechanistic explanation for this could be that the receptor-binding site of CCN2 domains III and IV is concealed by domains I and II as schematically depicted in Fig. 4*f*. Although no complete structure of any of the full-length CCN proteins has yet been reported, this would be in alignment with the structure proposed for CCN3 by Holbourn *et al.* (77) based on small-angle X-ray scattering. According to this structure, the individual domains of CCN proteins form extended molecules (77); such a structure would allow for the concealment of epitopes essential for receptor recognition and binding by the C-terminal domains III and IV.

This model also implies that the current attempts at targeting CCN2 with an antibody targeting domain II (10, 60, 62) rely on the blockage of activation of the preproprotein, *e.g.* through interfering with localization of CCN2 to membrane-bound proteases (46, 48, 49) or clearance of all body CCN2 (78). Whether inhibition of activation of CCN2 will be sufficient in disease states where soluble proteases are also often present remains to be seen. Ultimately, the structure of bioactive CCN2 and the mechanism of activation revealed here may facilitate studies on the role of CCN2 and other CCN proteins in pathophysiologic mechanisms of disease, the identification of recep-

tors mediating the signaling responses of CCN2 and other CCN proteins, and the development of drugs targeting and inhibiting the active part of CCN2 or other CCN proteins.

Experimental procedures

Plasmids

All plasmid constructs were generated by a combination of classical restriction endonuclease–based cloning, Gateway recombination cloning technology, and Gibson assembly. Plasmid maps of all destination vectors and inserts are shown in Fig. S6. All inserts were codon-optimized for human (biosensors) or hamster (recombinant CCN2 entities) expression and synthesized either as "DNA strings" or "gene synthesis" by Thermo Fisher Scientific (Waltham, MA), converted to entry vectors, and recombined with the destination vectors, as indicated in Fig. S6, to yield expression vectors. All constructs based on DNA strings were DNA sequence–verified (GATC Biotech, Constance, Germany), whereas constructs generated by gene synthesis were DNA sequence–verified by the manufacturer.

Protein production

FL-CCN2 was produced from DG44 CHO cells (a dihydrofolate reductase-deficient CHO cell line adapted for suspension culture) stably transfected with an expression vector encoding human CCN2 cDNA (GenBank™ accession number BC087839) and dihydrofolate reductase, allowing selection and amplification of CCN2 expression with methotrexate (subcloning and generation of cell line was performed by Fusion Antibodies Ltd. (Belfast, Ireland)). FL-CCN2 and fragments of CCN2 generated following secretion were all purified from the cell culture medium. For production of FL-CCN2, both monomer and dimer, 1×10^6/ml FL-CCN2–producing cells were seeded in shaker flasks in CD OptiCHO medium (Thermo Fisher Scientific (Gibco)). Following culture for 3 days (with rotatory shaking at 145 rpm), the cells were sedimented by centrifugation, and the cell culture medium was harvested. As prolonged culture (>3 days) increased the amounts of CCN2 entities of lower molecular mass, 1×10^6/ml CCN2-FL–producing cells were cultivated for 5 days (a time point when cell viability was still >95%) before harvest of cell culture medium for production and purification of CCN2-NT and CCN2-CT. For experiments with batimastat, parallel flasks of the FL-CCN2–producing cell line were seeded at a density of 0.5×10^6/ml with vehicle (0.1% DMSO) or batimastat (1 μM; Tocris Bioscience, UK) and cultured for 4 days before harvest of the cell culture medium. For d3-4-CCN2, a stable cell line was generated in suspension FreeStyle CHO-S cells (a CHO cell line adapted for suspension culture) with two rounds of puromycin selection (10 and 100 μg/ml) followed by limiting cell dilution to generate a stable single cell clone. To produce d3-4-CCN2, 1×10^6/ml cells of the stable clone were seeded in BalanCD CHO Growth A (Irvine Scientific) supplemented with 10 μg/ml puromycin and cultured for 4 days before harvest of the cell culture medium. For production of the fusion protein FL-CCN2–His–Halo–SUMO, a pool of stably selected DHFR$^{-/-}$ DG44 suspension CHO cells was generated by methotrexate amplification, and 1×10^6/ml cells were seeded in CD OptiCHO and cultivated for 4 days before harvest of the cell culture medium.

For production of FL-CCN1 and d3-4-CCN1, pools of stably selected DHFR$^{-/-}$ DG44 suspension CHO cells were generated by methotrexate amplification. For production of FL-CCN1, 1×10^6/ml FL-CCN1–producing cells were cultivated in shaker flasks in CD OptiCHO medium (Thermo Fisher Scientific (Gibco)) for 4 days before harvest. For production of d3-4-CCN1, 1×10^6/ml d3-4-CCN1–producing cells were maintained in shaker flasks (145 rpm) in ActiPro medium (GE Healthcare). After 3 days of culture, daily feeding with 4% (v/v) Cell Boost 7A and 0.4% (v/v) Cell Boost 7B (both from GE Healthcare) was implemented until harvest of the cell culture medium at day 6. All CHO suspension cells were cultured at 37 °C at 8% CO_2 unless noted otherwise.

For production of d3-4-CCN3, the ExpiCHO Max Titer protocol was utilized according to the manufacturer's procedure (Thermo Fisher Scientific). Briefly, 100 ml of ExpiCHO culture was transiently transfected with the d3-4-CCN3–encoding expression vector (for details, see Fig. S6*d*) before switching to 32 °C and an atmosphere with 5% CO_2 after 20 h. Supplements were added at days 1 and 5 as described in the manufacturer's protocol. The culture was harvested on day 7. Expression of FL-CCN3 in the ExpiCHO system did not yield any full-length product due to protease processing. All d3-4-CCN2–Fc fusions were produced utilizing the ExpiCHO manufacturer's Max Titer protocol as described above for d3-4-CCN3.

All harvesting of cell culture media was done while cell viability was >95%. At harvest, the media was clarified by centrifugation at 4750 × *g* for 20 min at 4 °C. Phenylmethylsulfonyl fluoride, EDTA, and MES buffer, pH 6.0, were added to all harvested cell culture media to give final concentrations of 1 mM phenylmethylsulfonyl fluoride, 0.5 mM EDTA, and 50 mM MES. The only exception was for purification of the Fc fragment (proteolytically cleaved from d3-4-CCN2–FL–Fc during cultivation) for which MES was replaced with Tris-HCl, pH 7.4, at a final concentration of 25 mM.

Protein purification

The purification procedures for all CCN2 entities (except the FL-CCN2–His–Halo–SUMO fusion protein) used for activity studies are depicted in Figs. S1 and S2. Fractions eluted from cationic ion-exchange chromatography columns were diluted in binding buffer to lower conductivity of the sample before heparin-Sepharose chromatography. FL-CCN1-M and d3-4-CCN1-M were purified using the same strategy as depicted in Fig. S2*a* for FL-CCN2-M and CT-CCN2, respectively. d3-4-CCN2–Fc fusion proteins and d3-4-CCN3-M were purified using the same strategy as for the untagged d3-4-CCN2 entities depicted in Fig. S2*b*. For the FL-CCN2–His–Halo–SUMO fusion protein, only a cationic ion-exchange chromatography step was used. For purification of the Fc fragment only, cell culture medium from the d3-4-CCN2–FL–Fc– expressing culture was subjected to protein A–Sepharose chromatography, which captured both the complete product (d3-4-CCN2–FL–Fc) and the Fc fragment with d3-4-CCN2 cleaved off. The Fc fragment was then separated from the d3-4–FL–Fc fusion protein by subsequent size-exclusion chromatography. All protein concentrations were determined with the micro-BCA method (Thermo Fisher Scientific). The chromatography media and

columns (all from GE Healthcare) and buffers (all chemicals from Sigma-Aldrich) used are listed in Table S1.

Cell lines

MCF-7 human mammary adenocarcinoma cells (ATCC HTB-22), Rat2 fibroblasts (ATCC CRL-1764), and murine RAW264.7 macrophage cells (ATCC TIB-71) were obtained from the American Type Culture Collection (LGC Standards, Germany). 293A, FreeStyle CHO-S, and CHO DG44 DHFR$^{-/-}$ were obtained from Thermo Fisher Scientific. MCF-7, Rat2, RAW264.7, and 293A were maintained in DMEM with high glucose (Gibco) supplemented with 10% fetal bovine serum and 50 μg/ml Gensumycin (Sanofi). FreeStyle CHO-S was maintained in FreeStyle CHO expression medium (Gibco) supplemented with 1× GlutaMAX (Gibco). CHO DG44 DHFR$^{-/-}$ was maintained in CD DG44 medium (Gibco) supplemented with 1× GlutaMAX (Gibco) and 0.18% Pluronic F-68 (Gibco) prior to transfection and either CD OptiCHO, BalanCD CHO Growth A, or ActiPro supplemented with puromycin or methotrexate as indicated above.

Antibodies

Anti-GAPDH (sc20357) and anti-CCN2 (L20 (sc14939)/E5 (sc365970)) antibodies were from Santa Cruz Biotechnology. Another anti-CCN2 IgG (ab6992) was from Abcam. Anti-SNAIL (C15D3), anti-E-cadherin (24E10) and anti-focal adhesion kinase (catalog number 3285) antibodies were from Cell Signaling Technology. Anti-vinculin IgG (catalog number V9264) was from Sigma-Aldrich. Secondary antibodies were from Santa Cruz Biotechnology (goat anti-mouse (sc2005) and donkey anti-goat (sc2056)) and GE Healthcare (donkey anti-rabbit (NA934V)).

Because the commercially available antibodies directed against domain III or IV of CCN2 were poor at detecting nonreduced CCN2, antiserum against CT-CCN2 was generated by immunization of rabbits performed by Eurogentec (Belgium). IgG from the antiserum was captured by protein A-Sepharose chromatography (GE Healthcare), and anti-CCN2 IgG was affinity-purified on a column packed with HaloLink Sepharose beads (Promega) coupled with FL-CCN2–His–Halo–SUMO and subsequently concentrated by ultrafiltration (Vivaspin 10,000 molecular weight cutoff, GE Healthcare). Chromatography media and columns were from GE Healthcare, and all other chemical were analytical grade from Sigma-Aldrich (listed in Table S1).

Western blot analysis and staining of SDS-polyacrylamide gels with Coomassie G-250

For experiments with MCF-7 cells, protein was extracted in a boiling lysis buffer composed of 1% SDS and 10 mM Tris-HCl, pH 8.8; sonicated; and centrifuged. Protein concentrations in the resulting supernatants were measured with a micro-BCA assay and adjusted accordingly. The MCF-7 cell extracts were separated on 8 or 12% polyacrylamide gels, whereas CCN2 protein preparations were separated on 4–15% TGX gradient gels (Bio-Rad). For Western blot analysis, proteins were transferred to PVDF membranes using the Trans-Blot Turbo semidry blotting system (Bio-Rad), and the membranes were blocked in 5% (w/v) nonfat dry milk dissolved in Tris-buffered saline with Tween 20 (20 mM Tris-HCl, pH 7.4, 140 mM NaCl, 2.5 mM KCl, and 0.1% Tween 20; all chemicals were analytical grade from Sigma-Aldrich) for 30–60 min before probing with primary antibody overnight at 4 °C. Secondary antibody incubation was performed at room temperature for 30–60 min before development with SuperSignal™ West Femto Maximum Sensitivity Substrate (Thermo Fisher Scientific) and analysis of chemiluminescence using the ChemiDoc imaging system (Bio-Rad). For Coomassie staining, gels were washed 3 × 5 min in water before staining with BioSafe G-250 Coomassie Stain (Bio-Rad) and destained with water. Coomassie-stained gels were imaged with the ChemiDoc imaging system.

MS analysis: Protein identification and Edman sequencing

FL-CCN2-D and NT-CCN2 were separated by SDS-PAGE, stained with Coomassie G-250, excised from the gel, and contract analyzed by nano-HPLC-ESI-MS/MS (Proteome Factory AG, Berlin, Germany). For Edman sequencing of CT-CCN2, SDS-PAGE–separated protein was transferred to a PVDF membrane with the Trans-Blot Turbo system, exchanging the standard manufacturer's blotting buffer with a buffer composed of 50 mM sodium borate, pH 9.0, in 20% methanol. To eliminate N-terminal blockage of the protein, the membrane was washed with deionized water and then incubated for 30 min at room temperature in 1% polyvinylpyrrolidone-40 in 0.1 M acetic acid. Subsequently, the membranes were washed three times (30 min each wash) in deionized water and then incubated overnight in PGAP buffer (manufacturer-supplied; Takara Biosciences) containing 50 milliunits of *Pfu* pyroglutamate aminopeptidase at 45 °C. Finally, the membranes were washed three times (15 min each wash) in deionized water and air-dried before analysis by Proteome Factory AG.

Identification of disulfide bridges of CCN2

In an attempt to identify the cysteines responsible for dimerization, d3-4-CCN2-M and d3-4-CCN2-D were subjected to LC-MS/MS analysis following the method described previously (33, 34). Briefly, after precipitation with 25% TCA on ice, the proteins were resuspended in 8 M urea and 100 mM Tris, pH 6.5, in the presence of 2 mM *N*-ethylmaleimide for Lys-C digestion. Then the samples were diluted 4-fold with 100 mM Tris-HCl, pH 6.5, containing 2 mM *N*-ethylmaleimide for further digestion with trypsin alone or trypsin and Glu-C. Peptide-*N*-glycosidase F (112 New England Biolabs units/6 μg of proteins) was added to remove glycans 2 h before the digestion was stopped. The resulting peptides were analyzed using an EASY-nLC 1000 system (Thermo Fisher Scientific) interfaced with a Q-Exactive HF mass spectrometer (Thermo Fisher Scientific). A 60-min reverse-phase gradient was used to separate peptides. The top 15 most intense precursor ions from each full scan (resolution, 60,000) were isolated for high-energy collisional dissociation MS2 (resolution, 15,000; normalized collision energy, 27) with a dynamic exclusion time of 30 s. The MS data were analyzed using pLink-SS, a software tool for identification of disulfide bridges as described in detail previously by Dong and co-workers (33, 34). This enables identification of disulfide

bridges but not differentiation of interprotein or intraprotein linkages.

Experimentally induced myocardial infarction in mice

All animal experiments were approved by the national board for animal research, permit number 6288, and were in accordance with the Guide for the Care and Use of Laboratory Animals published by the National Institutes of Health (publication number 85-23, revised 2010). Fourteen- to 16-week-old female C57BL/6JBomTac mice (Janvier Labs), with *ad libitum* access to food and water, were subjected to sham operation or myocardial infarction by ligation of the left anterior descending coronary artery (or not) as described previously by Gao *et al.* (79). Animals were euthanized 7 days after induction of myocardial infarction, the heart was excised, and granulation tissue from the infarcted left ventricle and nonischemic myocardial tissue were sampled.

2D electrophoresis and immunoblot analyses

For identification of CCN2 entities in granulation tissue from the infarct zone of mice subjected to myocardial infarction as well as in normal myocardial tissue from sham-operated mice ($n = 4$ animals/group), the tissue was crushed in liquid nitrogen and subsequently solubilized in buffer containing 1% SDS, 10 mM Tris-HCl, pH 8.8, 2 mM Na_3VO_4, 10 mM NaF, 4 mM β-glycerophosphate, and 4 mM pyrophosphate. Extracts were then subjected or not to deglycosylation, utilizing Protein Deglycosylation Mix II (New England Biolabs). Extracts were then subjected initially to first dimension electrophoresis on immobilized pH gradient strips (pI range, 7–10; Bio-Rad). Following isoelectric focusing, second dimension electrophoresis was performed on 12% acrylamide gels before semidry blotting (as described above) and detection with anti-CCN2 antibody. A similar protocol was used for investigation of glycosylation of fractions collected from FPLC.

AKT, ERK, S6K, RSK, and Rac1 biosensor assays

Plasmids encoding for the various biosensors were generated as described under "Plasmids" and in Fig. S6 and introduced into Rat2 or MCF-7 cells by electroporation (Neon transfection system, Thermo Fisher Scientific) using manufacturer-developed parameters for NIH3T3 or MCF-7, respectively. For generation of stable cell lines, electroporated Rat2 cells were maintained in 5 μg/ml puromycin and MCF-7 cells were maintained in 0.25 μg/ml puromycin until the appearance of isolated colonies, which were expanded and tested for signal intensity. The cell clones with the highest expression levels and preserved cell proliferation were subsequently maintained in 2.5 (Rat2 cells) or 0.1 μg/ml (MCF-7 cells) puromycin. For assays, 10,000 cells/well were seeded in white-walled 96-well cell culture plates, maintained in a CO_2 incubator overnight, and subsequently changed to CO_2-Independent™ medium (Gibco) without serum. After 5–6 h of serum starvation, 10% (v/v) NanoGlo Live Cell reagent (Promega) was added, and relative light unit measurements were started in a PolarStar Omega plate reader (BMG Labtech, Germany). After 15 min of stabilization, the measurements were paused, and protein preparations were added with a multichannel pipette before continuing the measurements for 30 min. The values from all wells were background-normalized to their individual prestimulatory values (recorded during the last 3 min before stimulation) and then to the vehicle control values. The area under the curve (AUC) for the 30 min after stimulation was calculated for each individual well using GraphPad Prism 6. This conversion to a single value from continuous recordings was performed to enable unbiased comparison of the potencies of different protein preparations. For the concentration-effect curves, protein concentrations were converted to molar units based on calculated molecular weights (subtracting the signal peptide) for unprocessed entities and MS-mapped sequences for the processed CCN2 entities. To enable comparison of results from multiple experiments, the AUC values were expressed as the percentage of the response of the positive control, 0.5 μg/ml EGF (R&D Systems, catalog number 236-EG), which was included in all experiments. For the experiments with activity testing after MMP8 digestion of FL-CCN2-M, the AUC from the cutting reactions with batimastat added 2 h after MMP8 were related directly to the reactions with batimastat added before incubation with MMP8. All inhibitors used for the validation of the biosensors (API-2, AKTi1/2, U0126, SL327, rapamycin, and BI-D1870) were from Tocris (UK).

TGFβ/SMAD reporter assay

A shuttle vector, compatible with the RAPAd adenoviral expression system (Cell Biolabs), with four SMAD-binding response elements (4SBE) controlling the expression of firefly luciferase was generated as illustrated in Fig. S6 and used to produce adenovirus by cotransfecting 293A cells together with the RAPAd viral backbone vector. The virus was purified by CaptoCore700 HiTrap column chromatography (GE Healthcare) and titered with the Adeno-X Rapid Titer kit from Clontech (Takara Bio). Rat2 cells were seeded at a density of 10,000 cells/well, transduced with adenovirus encoding the 4SBE reporter at a multiplicity of infection of 1000, and incubated overnight before serum starvation. After 16–20 h of serum starvation, the cells were stimulated for 24 h after which the medium was decanted, and 100 μl of ONE-Glo substrate/lysis reagent (Promega), diluted 1:4 in H_2O, was added to each well. The plates were then incubated for 10 min before the lysate was transferred to black-walled plates, and luciferase activity was determined by recording luminescence with the PolarStar Omega plate reader.

Immunoassay of phosphoproteins

Rat2 cells were seeded at a density of 350,000/well in 6-well plates and serum-starved for 16–20 h before stimulation with the various CCN2 entities for 20 min. The cells were subsequently lysed in BioPlex lysis buffer (Bio-Rad), corrected for protein content (micro-BCA assay), and analyzed with Luminex bead–based immunoassays (BioPlex immunoassays, Bio-Rad) of phospho-AKT (Ser^{473}) and phospho-ERK1/2 (Thr^{202}/Tyr^{204} and Thr^{185}/Tyr^{187}) according to the manufacturer's instructions. Briefly, the phosphoproteins of interest were captured with antibody-coupled beads and labeled with a second antibody coupled to a fluorophore, enabling analysis with the BioPlex 200 instrument (Bio-Rad).

Cell migration assay

To test the effect of various CCN2 entities on cell migration, the transwell migration assay (Thermo Fisher Scientific) (also known as a modified Boyden chamber assay) was used. Cells were seeded on top of a 5-μm-pore-diameter PVDF membrane containing transwells in serum-free medium. CCN2 test fractions were added to the lower chamber of the transwells. Following a 16-h incubation, Cell-ROX dye (Invitrogen, catalog number C10422) was added to the lower chamber to stain migrated cells. Following a 10-min incubation, the top chamber was scraped to remove unmigrated cells. The membranes were then removed from the chamber, immobilized on glass slides, and used for imaging on a Zeiss Axio Observer Z.1 imaging system. Images were analyzed in Adobe Photoshop CC by an investigator blinded to the experimental groups. Results of the migration assays are expressed as the percentage of seeded cells migrated to the lower chamber.

Focal adhesion complex formation

Rat2 fibroblasts were seeded on an eight-chamber glass slide and following overnight serum starvation were stimulated with various CCN2 entities for 24 h. The cells were subsequently fixed with 4% paraformaldehyde in PBS and immunostained for focal adhesion kinase (Cell Signaling Technology, catalog number 3285) and vinculin (Sigma, catalog number V9264) before counterstaining with DAPI. The entirety of cell volume was acquired as Z-stacks (of thickness 0.5 μm) with a Zeiss Axio Observer Z.1 imaging system. Images were analyzed in ImageJ (National Institutes of Health, Bethesda, MD) by an investigator blinded to the experimental groups. Individual cell boundaries were defined as visible from the localization of complexes or based on a distance of 10 μm from the nucleus boundary (DAPI staining). Results are expressed as the number of focal adhesion complexes (spots with overlapping signals for focal adhesion kinase and vinculin) per cell. Data are mean ± S.E. of three independent experiments per group/condition (a total of 250 cells were analyzed per experimental condition).

Cell proliferation assays

Rat2 cells were seeded in 96-well plates at a density of 3000 cells/well and allowed to settle overnight. Cells were then serum-starved for 16–20 h before stimulation with the various protein preparations. After 48 h, the cells were analyzed with the CellTiter-Glo assay system (Promega) according to the manufacturer's instructions. Results are expressed as the percentage of vehicle control values. For BrdU analysis of DNA synthesis (Roche Applied Science, chemiluminescent ELISA BrdU kit), the cells were labeled with BrdU for 2 h after either 48- or 72-h stimulation with various CCN2 entities. BrdU incorporation was subsequently determined according to the manufacturer's instructions. Both the CellTiter-Glo and BrdU assays were recorded with a PerkinElmer Life Sciences Victor X5 plate reader.

Mammosphere assay

Single-cell suspensions of MCF-7 cells were generated by trypsinization of adherent MCF-7 cultures followed by trituration through a 25-gauge needle five times and filtering through a 40-μm cell filter prior to seeding at density of 200 cells/well in 96-well ultralow-adhesion plates (Sarstedt) in DMEM/F-12 supplemented with B27 without vitamin A (both from Gibco). Cells were then incubated with or without indicated protein preparations for 7 or 10 days, stained with thiazolyl blue tetrazolium bromide (3-(4,5-dimethylthiazol-2-yl)-2,5-diphenyltetrazolium bromide (MTT); Sigma-Aldrich). Spheres were semiautomatically quantified (40-μm-diameter cutoff) with the Oxford Optronix Gelcount^{TM} system.

Tartrate-resistant acid phosphatase (TRAP) assay

RAW264.7 cells were seeded at a density of 10,000 cells/well in DMEM supplemented with 0.5% fetal calf serum and 1 μg/ml d3-4-CCN2-D for 7 days before staining with the TRAP kit from Clontech (Takara Bio). TRAP-positive cells (stained cells) were visualized by light microscopy with a digital camera (Zeiss Axiovert A1 connected to AxioCam ERc5s), and images were acquired and analyzed with Adobe Photoshop 3.0 and quantified as positive cells/field of view with 20× magnification. For each experiment, two wells were utilized for each condition, and three images were taken per well at the areas of maximal cell density.

MMP 30F-PALA-AYRLE biosensor assay

A protease sensor for the ^{177}PALAAYRLE^{185} part of CCN2 was generated by inserting the ^{177}PALAAYRLE^{185} sequence into the protease site of a protease biosensor based on a circularly permuted *Photuris pennsylvanica* luciferase (80) (provided as 30F by Promega). The signal peptide of human albumin was appended to the N terminus, and the resulting protease biosensor, 30F-PALA-AYRLE, was codon-optimized for Chinese hamster and expressed in FreeStyle CHO S cells. After selection of stably transfected cells with 10 μg/ml puromycin, the cells were seeded in fresh cell culture medium at a density of 1 × 10^6/ml and cultured for 4 days. The cell culture medium was subsequently harvested and stored at −70 °C until use. For assaying MMP activity, 95 μl of freshly thawed cell culture medium (containing the secreted 30F-PALA-AYRLE biosensor) admixed with 2 μl of cAMP reagent (Promega) was distributed in black-walled 96-well plates, and luminescence was recorded with the PolarStar Omega plate reader. Active domains of recombinant MMPs (Enzo Life Sciences) were added (0.25 μg/well) after 5 min, and the signals were monitored for an additional 40 min. To enable statistical comparisons, the continuous recordings were converted to a single value by calculating the AUC for the last 15 min of the assay, when all the MMP reactions had reached plateaus, with GraphPad Prism 6.

MMP cleavage of recombinant CCN2

FL-CCN2-M (final concentration of 1.0 μg/10 μl) was incubated with 1× MMP buffer and recombinant MMPs (final concentration of 80 ng/10 μl) with 1 μM batimastat added either before MMP addition or 2 h after MMP addition. The MMP buffer consisted of 50 mM HEPES, pH 7.0, 10 mM $CaCl_2$, 0.05% Brij 35, and 150 mM NaCl; for MMP3, the HEPES was exchanged with 50 mM MES, pH 6.0, according to the manufa-

cturer's instructions. For the experiments with subsequent activity testing, the final concentration of FL-CCN2-M was 24 μg/ml (*i.e.* 12 μg/ml each part if FL-CCN2-M was cut right in the middle), and Brij 35 was omitted from the MMP buffer to avoid cell lysis.

Statistical analysis

The number of independent experiments and which statistical methods were used for comparisons are described in the respective figure legends. Error bars in the figures indicate S.E. All statistical comparisons, except for the analysis of the MS data, were performed with GraphPad Prism 6. For comparison of two experimental groups, unpaired Student's two-tailed *t* test was used. For comparison of several experimental groups, one-way ANOVA was used followed by Dunnett's post hoc test when the experimental groups were only compared with the control group (protease biosensor experiments) to avoid comparison with an unrepresentative intergroup mean, whereas Šidák's post hoc test was used when experimental groups were compared with both vehicle control and FL-CCN2-M and for kinase biosensor validation experiments in which more than one pharmacological inhibitor was utilized. Statistical significance ($p < 0.05$) for performed tests is indicated in the figures.

Data availability

All source data used to generate graphs in this report are available from the corresponding author upon request.

Author contributions—O. J. K. and H. A. conceptualization; O. J. K., A. K. G., J.-H. W., V. T. M., and E. M. V. H. data curation; O. J. K., A. K. G., J.-H. W., and E. M. V. H. formal analysis; O. J. K., M.-Q. D., and H. A. supervision; O. J. K., A. K. G., J.-H. W., V. T. M., E. M. V. H., and M.-Q. D. investigation; O. J. K., A. K. G., J.-H. W., V. T. M., and M.-Q. D. visualization; O. J. K., A. K. G., J.-H. W., V. T. M., E. M. V. H., M.-Q. D., and H. A. methodology; O. J. K. and H. A. writing-original draft; O. J. K. and H. A. project administration; O. J. K., A. K. G., J.-H. W., V. T. M., E. M. V. H., M.-Q. D., and H. A. writing-review and editing; H. A. resources; H. A. funding acquisition.

Acknowledgment—We thank Dr. Lester F. Lau, University of Illinois at Chicago, for advice and for critically reading the manuscript.

References

1. Jun, J.-I., and Lau, L. F. (2011) Taking aim at the extracellular matrix: CCN proteins as emerging therapeutic targets. *Nat. Rev. Drug Discov.* **10,** 945–963 CrossRef Medline
2. Schafer, S., Viswanathan, S., Widjaja, A. A., Lim, W. W., Moreno-Moral, A., DeLaughter, D. M., Ng, B., Patone, G., Chow, K., Khin, E., Tan, J., Chothani, S. P., Ye, L., Rackham, O. J. L., Ko, N. S. J., *et al.* (2017) IL-11 is a crucial determinant of cardiovascular fibrosis. *Nature* **552,** 110–115 CrossRef Medline
3. Nishida, Y., Yoshioka, M., and St-Amand, J. (2005) The top 10 most abundant transcripts are sufficient to characterize the organs functional specificity: evidences from the cortex, hypothalamus and pituitary gland. *Gene* **344,** 133–141 CrossRef Medline
4. Rachfal, A. W., and Brigstock, D. R. (2005) Structural and functional properties of CCN proteins. *Vitam. Horm.* **70,** 69–103 CrossRef Medline
5. Leask, A., and Abraham, D. J. (2006) All in the CCN family: essential matricellular signaling modulators emerge from the bunker. *J. Cell Sci.* **119,** 4803–4810 CrossRef Medline
6. Murphy-Ullrich, J. E., and Sage, E. H. (2014) Revisiting the matricellular concept. *Matrix Biol.* **37,** 1–14 CrossRef Medline
7. Lau, L. F. (2016) Cell surface receptors for CCN proteins. *J. Cell Commun. Signal.* **10,** 121–127 CrossRef Medline
8. Tong, Z., Chen, R., Alt, D. S., Kemper, S., Perbal, B., and Brigstock, D. R. (2009) Susceptibility to liver fibrosis in mice expressing a connective tissue growth factor transgene in hepatocytes. *Hepatology* **50,** 939–947 CrossRef Medline
9. Ahmed, M. S., Gravning, J., Martinov, V. N., von Lueder, T. G., Edvardsen, T., Czibik, G., Moe, I. T., Vinge, L. E., Øie, E., Valen, G., and Attramadal, H. (2011) Mechanisms of novel cardioprotective functions of CCN2/CTGF in myocardial ischemia-reperfusion injury. *Am. J. Physiol. Heart Circ. Physiol.* **300,** H1291–H1302 CrossRef Medline
10. Neesse, A., Frese, K. K., Bapiro, T. E., Nakagawa, T., Sternlicht, M. D., Seeley, T. W., Pilarsky, C., Jodrell, D. I., Spong, S. M., and Tuveson, D. A. (2013) CTGF antagonism with mAb FG-3019 enhances chemotherapy response without increasing drug delivery in murine ductal pancreas cancer. *Proc. Natl. Acad. Sci. U.S.A.* **110,** 12325–12330 CrossRef Medline
11. Ball, D. K., Surveyor, G. A., Diehl, J. R., Steffen, C. L., Uzumcu, M., Mirando, M. A., and Brigstock, D. R. (1998) Characterization of 16-to 20-kilodalton (kDa) connective tissue growth factors (CTGFs) and demonstration of proteolytic activity for 38-kDa CTGF in pig uterine luminal flushings. *Biol. Reprod.* **59,** 828–835 CrossRef Medline
12. Robinson, P. M., Smith, T. S., Patel, D., Dave, M., Lewin, A. S., Pi, L., Scott, E. W., Tuli, S. S., and Schultz, G. S. (2012) Proteolytic processing of connective tissue growth factor in normal ocular tissues and during corneal wound healing. *Invest. Ophthalmol. Vis. Sci.* **53,** 8093–8103 CrossRef Medline
13. Heng, E. C., Huang, Y., Black, S. A., Jr., and Trackman, P. C. (2006) CCN2, connective tissue growth factor, stimulates collagen deposition by gingival fibroblasts via module 3 and α6- and β1 integrins. *J. Cell. Biochem.* **98,** 409–420 CrossRef Medline
14. Ball, D. K., Moussad, E. E., Rageh, M. A., Kemper, S. A., and Brigstock, D. R. (2003) Establishment of a recombinant expression system for connective tissue growth factor (CTGF) that models CTGF processing in utero. *Reproduction* **125,** 271–284 CrossRef Medline
15. Ball, D. K., Rachfal, A. W., Kemper, S. A., and Brigstock, D. R. (2003) The heparin-binding 10 kDa fragment of connective tissue growth factor (CTGF) containing module 4 alone stimulates cell adhesion. *J. Endocrinol.* **176,** R1–7 CrossRef Medline
16. Steffen, C. L., Ball-Mirth, D. K., Harding, P. A., Bhattacharyya, N., Pillai, S., and Brigstock, D. R. (1998) Characterization of cell-associated and soluble forms of connective tissue growth factor (CTGF) produced by fibroblast cells *in vitro*. *Growth Factors* **15,** 199–213 CrossRef Medline
17. Brigstock, D. R., Steffen, C. L., Kim, G. Y., Vegunta, R. K., Diehl, J. R., and Harding, P. A. (1997) Purification and characterization of novel heparin-binding growth factors in uterine secretory fluids. Identification as heparin-regulated M_r 10,000 forms of connective tissue growth factor. *J. Biol. Chem.* **272,** 20275–20282 CrossRef Medline
18. Lin, C. H., Yu, M. C., Tung, W. H., Chen, T. T., Yu, C. C., Weng, C. M., Tsai, Y. J., Bai, K. J., Hong, C. Y., Chien, M. H., and Chen, B. C. (2013) Connective tissue growth factor induces collagen I expression in human lung fibroblasts through the Rac1/MLK3/JNK/AP-1 pathway. *Biochim. Biophys. Acta* **1833,** 2823–2833 CrossRef Medline
19. Moe, I. T., Pham, T. A., Hagelin, E. M., Ahmed, M. S., and Attramadal, H. (2013) CCN2 exerts direct cytoprotective actions in adult cardiac myocytes by activation of the PI3-kinase/Akt/GSK-3β signaling pathway. *J. Cell Commun. Signal.* **7,** 31–47 CrossRef Medline
20. Johnson, B. G., Ren, S., Karaca, G., Gomez, I. G., Fligny, C., Smith, B., Ergun, A., Locke, G., Gao, B., Hayes, S., MacDonnell, S., and Duffield, J. S. (2017) Connective tissue growth factor domain 4 amplifies fibrotic kidney disease through activation of LDL receptor-related protein 6. *J. Am. Soc. Nephrol.* **28,** 1769–1782 CrossRef Medline
21. Mokalled, M. H., Patra, C., Dickson, A. L., Endo, T., Stainier, D. Y., and Poss, K. D. (2016) Injury-induced *ctgfa* directs glial bridging and spinal cord regeneration in zebrafish. *Science* **354,** 630–634 CrossRef Medline
22. Robertson, I. B., and Rifkin, D. B. (2013) Unchaining the beast; insights from structural and evolutionary studies on TGFβ secretion, sequestra-

tion, and activation. *Cytokine Growth Factor Rev.* **24,** 355–372 CrossRef Medline
23. Weathington, N. M., van Houwelingen, A. H., Noerager, B. D., Jackson, P. L., Kraneveld, A. D., Galin, F. S., Folkerts, G., Nijkamp, F. P., and Blalock, J. E. (2006) A novel peptide CXCR ligand derived from extracellular matrix degradation during airway inflammation. *Nat. Med.* **12,** 317–323 CrossRef Medline
24. Sage, E. H., Reed, M., Funk, S. E., Truong, T., Steadele, M., Puolakkainen, P., Maurice, D. H., and Bassuk, J. A. (2003) Cleavage of the matricellular protein SPARC by matrix metalloproteinase 3 produces polypeptides that influence angiogenesis. *J. Biol. Chem.* **278,** 37849–37857 CrossRef Medline
25. Takafuji, V., Forgues, M., Unsworth, E., Goldsmith, P., and Wang, X. W. (2007) An osteopontin fragment is essential for tumor cell invasion in hepatocellular carcinoma. *Oncogene* **26,** 6361–6371 CrossRef Medline
26. Tan, T. K., Zheng, G., Hsu, T. T., Lee, S. R., Zhang, J., Zhao, Y., Tian, X., Wang, Y., Wang, Y. M., Cao, Q., Wang, Y., Lee, V. W., Wang, C., Zheng, D., Alexander, S. I., *et al*. (2013) Matrix metalloproteinase-9 of tubular and macrophage origin contributes to the pathogenesis of renal fibrosis via macrophage recruitment through osteopontin cleavage. *Lab. Invest.* **93,** 434–449 CrossRef Medline
27. Bohr, W., Kupper, M., Hoffmann, K., and Weiskirchen, R. (2010) Recombinant expression, purification, and functional characterisation of connective tissue growth factor and nephroblastoma-overexpressed protein. *PLoS One* **5,** e16000 CrossRef Medline
28. Hashimoto, G., Inoki, I., Fujii, Y., Aoki, T., Ikeda, E., and Okada, Y. (2002) Matrix metalloproteinases cleave connective tissue growth factor and reactivate angiogenic activity of vascular endothelial growth factor 165. *J. Biol. Chem.* **277,** 36288–36295 CrossRef Medline
29. Miura, H., Matsuda, M., and Aoki, K. (2014) Development of a FRET biosensor with high specificity for Akt. *Cell Struct. Funct.* **39,** 9–20 CrossRef Medline
30. Dixon, A. S., Schwinn, M. K., Hall, M. P., Zimmerman, K., Otto, P., Lubben, T. H., Butler, B. L., Binkowski, B. F., Machleidt, T., Kirkland, T. A., Wood, M. G., Eggers, C. T., Encell, L. P., and Wood, K. V. (2016) NanoLuc complementation reporter optimized for accurate measurement of protein interactions in cells. *ACS Chem. Biol.* **11,** 400–408 CrossRef Medline
31. Ahmed, M. S., Øie, E., Vinge, L. E., Yndestad, A., Øystein Andersen, G., Andersson, Y., Attramadal, T., and Attramadal, H. (2004) Connective tissue growth factor—a novel mediator of angiotensin II-stimulated cardiac fibroblast activation in heart failure in rats. *J. Mol. Cell. Cardiol.* **36,** 393–404 CrossRef Medline
32. Bork, P. (1993) The modular architecture of a new family of growth regulators related to connective tissue growth factor. *FEBS Lett.* **327,** 125–130 CrossRef Medline
33. Lu, S., Fan, S. B., Yang, B., Li, Y. X., Meng, J. M., Wu, L., Li, P., Zhang, K., Zhang, M. J., Fu, Y., Luo, J., Sun, R. X., He, S. M., and Dong, M. Q. (2015) Mapping native disulfide bonds at a proteome scale. *Nat. Methods* **12,** 329–331 CrossRef Medline
34. Lu, S., Cao, Y., Fan, S. B., Chen, Z. L., Fang, R. Q., He, S. M., and Dong, M. Q. (2018) Mapping disulfide bonds from sub-micrograms of purified proteins or micrograms of complex protein mixtures. *Biophys. Rep.* **4,** 68–81 CrossRef Medline
35. Crean, J. K., Finlay, D., Murphy, M., Moss, C., Godson, C., Martin, F., and Brady, H. R. (2002) The role of p42/44 MAPK and protein kinase B in connective tissue growth factor induced extracellular matrix protein production, cell migration, and actin cytoskeletal rearrangement in human mesangial cells. *J. Biol. Chem.* **277,** 44187–44194 CrossRef Medline
36. Lee, C. H., Lee, F. Y., Tarafder, S., Kao, K., Jun, Y., Yang, G., and Mao, J. J. (2015) Harnessing endogenous stem/progenitor cells for tendon regeneration. *J. Clin. Investig.* **125,** 2690–2701 CrossRef Medline
37. Chen, C. C., Chen, N., and Lau, L. F. (2001) The angiogenic factors Cyr61 and connective tissue growth factor induce adhesive signaling in primary human skin fibroblasts. *J. Biol. Chem.* **276,** 10443–10452 CrossRef Medline
38. Chien, W., O'Kelly, J., Lu, D., Leiter, A., Sohn, J., Yin, D., Karlan, B., Vadgama, J., Lyons, K. M., and Koeffler, H. P. (2011) Expression of connective tissue growth factor (CTGF/CCN2) in breast cancer cells is associated with increased migration and angiogenesis. *Int. J. Oncol.* **38,** 1741–1747 CrossRef Medline
39. Hishikawa, K., Oemar, B. S., Tanner, F. C., Nakaki, T., Lüscher, T. F., and Fujii, T. (1999) Connective tissue growth factor induces apoptosis in human breast cancer cell line MCF-7. *J. Biol. Chem.* **274,** 37461–37466 CrossRef Medline
40. Tomasek, J. J., Gabbiani, G., Hinz, B., Chaponnier, C., and Brown, R. A. (2002) Myofibroblasts and mechano-regulation of connective tissue remodelling. *Nat. Rev. Mol. Cell Biol.* **3,** 349–363 CrossRef Medline
41. Jun, J. I., and Lau, L. F. (2017) CCN2 induces cellular senescence in fibroblasts. *J. Cell Commun. Signal.* **11,** 15–23 CrossRef Medline
42. Nishida, T., Emura, K., Kubota, S., Lyons, K. M., and Takigawa, M. (2011) CCN family 2/connective tissue growth factor (CCN2/CTGF) promotes osteoclastogenesis via induction of and interaction with dendritic cell-specific transmembrane protein (DC-STAMP). *J. Bone Miner. Res.* **26,** 351–363 CrossRef Medline
43. Zhu, X., Zhong, J., Zhao, Z., Sheng, J., Wang, J., Liu, J., Cui, K., Chang, J., Zhao, H., and Wong, S. (2015) Epithelial derived CTGF promotes breast tumor progression via inducing EMT and collagen I fibers deposition. *Oncotarget* **6,** 25320–25338 CrossRef Medline
44. Pi, L., Jorgensen, M., Oh, S. H., Protopapadakis, Y., Gjymishka, A., Brown, A., Robinson, P., Liu, C., Scott, E. W., Schultz, G. S., and Petersen, B. E. (2015) A disintegrin and metalloprotease with thrombospondin type I motif 7: a new protease for connective tissue growth factor in hepatic progenitor/oval cell niche. *Am. J. Pathol.* **185,** 1552–1563 CrossRef Medline
45. Guillon-Munos, A., Oikonomopoulou, K., Michel, N., Smith, C. R., Petit-Courty, A., Canepa, S., Reverdiau, P., Heuzé-Vourc'h, N., Diamandis, E. P., and Courty, Y. (2011) Kallikrein-related peptidase 12 hydrolyzes matricellular proteins of the CCN family and modifies interactions of CCN1 and CCN5 with growth factors. *J. Biol. Chem.* **286,** 25505–25518 CrossRef Medline
46. Mochizuki, S., Tanaka, R., Shimoda, M., Onuma, J., Fujii, Y., Jinno, H., and Okada, Y. (2010) Connective tissue growth factor is a substrate of ADAM28. *Biochem. Biophys. Res. Commun.* **402,** 651–657 CrossRef Medline
47. Dean, R. A., Butler, G. S., Hamma-Kourbali, Y., Delbé, J., Brigstock, D. R., Courty, J., and Overall, C. M. (2007) Identification of candidate angiogenic inhibitors processed by matrix metalloproteinase 2 (MMP-2) in cell-based proteomic screens: disruption of vascular endothelial growth factor (VEGF)/heparin affin regulatory peptide (pleiotrophin) and VEGF/Connective tissue growth factor angiogenic inhibitory complexes by MMP-2 proteolysis. *Mol. Cell. Biol.* **27,** 8454–8465 CrossRef Medline
48. Butler, G. S., Connor, A. R., Sounni, N. E., Eckhard, U., Morrison, C. J., Noël, A., and Overall, C. M. (2017) Degradomic and yeast 2-hybrid inactive catalytic domain substrate trapping identifies new membrane-type 1 matrix metalloproteinase (MMP14) substrates: CCN3 (Nov) and CCN5 (WISP2). *Matrix Biol.* **59,** 23–38 CrossRef Medline
49. Tam, E. M., Morrison, C. J., Wu, Y. I., Stack, M. S., and Overall, C. M. (2004) Membrane protease proteomics: isotope-coded affinity tag MS identification of undescribed MT1-matrix metalloproteinase substrates. *Proc. Natl. Acad. Sci. U.S.A.* **101,** 6917–6922 CrossRef Medline
50. Canfield, S. M., and Morrison, S. L. (1991) The binding affinity of human IgG for its high affinity Fc receptor is determined by multiple amino acids in the CH2 domain and is modulated by the hinge region. *J. Exp. Med.* **173,** 1483–1491 CrossRef Medline
51. Glaesner, W., Vick, A. M., Millican, R., Ellis, B., Tschang, S. H., Tian, Y., Bokvist, K., Brenner, M., Koester, A., Porksen, N., Etgen, G., and Bumol, T. (2010) Engineering and characterization of the long-acting glucagon-like peptide-1 analogue LY2189265, an Fc fusion protein. *Diabetes Metab. Res. Rev.* **26,** 287–296 CrossRef Medline
52. Hecht, R., Li, Y. S., Sun, J., Belouski, E., Hall, M., Hager, T., Yie, J., Wang, W., Winters, D., Smith, S., Spahr, C., Tam, L. T., Shen, Z., Stanislaus, S., Chinookoswong, N., *et al.* (2012) Rationale-based engineering of a potent long-acting FGF21 analog for the treatment of type 2 diabetes. *PLoS One* **7,** e49345 CrossRef Medline
53. Weng, Y., Ishino, T., Sievers, A., Talukdar, S., Chabot, J. R., Tam, A., Duan, W., Kerns, K., Sousa, E., He, T., Logan, A., Lee, D., Li, D., Zhou, Y., Ber-

nardo, B., *et al.* (2018) Glyco-engineered long acting FGF21 variant with optimal pharmaceutical and pharmacokinetic properties to enable weekly to twice monthly subcutaneous dosing. *Sci. Rep.* **8,** 4241 CrossRef Medline
54. Almendral, J. M., Sommer, D., Macdonald-Bravo, H., Burckhardt, J., Perera, J., and Bravo, R. (1988) Complexity of the early genetic response to growth factors in mouse fibroblasts. *Mol. Cell. Biol.* **8,** 2140–2148 CrossRef Medline
55. Cunningham, B. C., Mulkerrin, M. G., and Wells, J. A. (1991) Dimerization of human growth hormone by zinc. *Science* **253,** 545–548 CrossRef Medline
56. Wang, X., Fischer, G., and Hyvönen, M. (2016) Structure and activation of pro-activin A. *Nat. Commun.* **7,** 12052 CrossRef Medline
57. Gray, A. M., and Mason, A. J. (1990) Requirement for activin A and transforming growth factor-β1 pro-regions in homodimer assembly. *Science* **247,** 1328–1330 CrossRef Medline
58. Chen, N., Leu, S. J., Todorovic, V., Lam, S. C., and Lau, L. F. (2004) Identification of a novel integrin $\alpha v\beta 3$ binding site in CCN1 (CYR61) critical for pro-angiogenic activities in vascular endothelial cells. *J. Biol. Chem.* **279,** 44166–44176 CrossRef Medline
59. Babic, A. M., Chen, C. C., and Lau, L. F. (1999) Fisp12/mouse connective tissue growth factor mediates endothelial cell adhesion and migration through integrin $\alpha v\beta 3$, promotes endothelial cell survival, and induces angiogenesis in vivo. *Mol. Cell. Biol.* **19,** 2958–2966 CrossRef Medline
60. Morales, M. G., Gutierrez, J., Cabello-Verrugio, C., Cabrera, D., Lipson, K. E., Goldschmeding, R., and Brandan, E. (2013) Reducing CTGF/CCN2 slows down *mdx* muscle dystrophy and improves cell therapy. *Hum. Mol. Gen.* **22,** 4938–4951 CrossRef Medline
61. Bickelhaupt, S., Erbel, C., Timke, C., Wirkner, U., Dadrich, M., Flechsig, P., Tietz, A., Pföhler, J., Gross, W., Peschke, P., Hoeltgen, L., Katus, H. A., Gröne, H. J., Nicolay, N. H., Saffrich, R., *et al.* (2017) Effects of CTGF blockade on attenuation and reversal of radiation-induced pulmonary fibrosis. *J. Natl. Cancer Inst.* **109,** djw339 CrossRef Medline
62. Raghu, G., Scholand, M. B., de Andrade, J., Lancaster, L., Mageto, Y., Goldin, J., Brown, K. K., Flaherty, K. R., Wencel, M., Wanger, J., Neff, T., Valone, F., Stauffer, J., and Porter, S. (2016) FG-3019 anti-connective tissue growth factor monoclonal antibody: results of an open-label clinical trial in idiopathic pulmonary fibrosis. *Eur. Respir. J.* **47,** 1481–1491 CrossRef Medline
63. Aoyama, E., Hattori, T., Hoshijima, M., Araki, D., Nishida, T., Kubota, S., and Takigawa, M. (2009) N-terminal domains of CCN family 2/connective tissue growth factor bind to aggrecan. *Biochem. J.* **420,** 413–420 CrossRef Medline
64. Abreu, J. G., Ketpura, N. I., Reversade, B., and De Robertis, E. (2002) Connective-tissue growth factor (CTGF) modulates cell signalling by BMP and TGF-β. *Nat. Cell Biol.* **4,** 599–604 CrossRef Medline
65. Xu, E. R., Blythe, E. E., Fischer, G., and Hyvönen, M. (2017) Structural analyses of von Willebrand factor C domains of collagen 2A and CCN3 reveal an alternative mode of binding to bone morphogenetic protein-2. *J. Biol. Chem.* **292,** 12516–12527 CrossRef Medline
66. Grotendorst, G. R., and Duncan, M. R. (2005) Individual domains of connective tissue growth factor regulate fibroblast proliferation and myofibroblast differentiation. *FASEB J.* **19,** 729–738 CrossRef Medline
67. Yang, Z., Sun, Z., Liu, H., Ren, Y., Shao, D., Zhang, W., Lin, J., Wolfram, J., Wang, F., and Nie, S. (2015) Connective tissue growth factor stimulates the proliferation, migration and differentiation of lung fibroblasts during paraquat-induced pulmonary fibrosis. *Mol. Med. Rep.* **12,** 1091–1097 CrossRef Medline
68. Roopenian, D. C., and Akilesh, S. (2007) FcRn: the neonatal Fc receptor comes of age. *Nat. Rev. Immunol* **7,** 715–725 CrossRef Medline
69. Schütze, N., Kunzi-Rapp, K., Wagemanns, R., Nöth, U., Jatzke, S., and Jakob, F. (2005) Expression, purification, and functional testing of recombinant CYR61/CCN1. *Protein Expr. Purif.* **42,** 219–225 CrossRef Medline
70. Schütze, N., Schenk, R., Fiedler, J., Mattes, T., Jakob, F., and Brenner, R. E. (2007) CYR61/CCN1 and WISP3/CCN6 are chemoattractive ligands for human multipotent mesenchymal stroma cells. *BMC Cell Biol.* **8,** 45 CrossRef Medline
71. Su, B. Y., Cai, W. Q., Zhang, C. G., Martinez, V., Lombet, A., and Perbal, B. (2001) The expression of ccn3 (nov) RNA and protein in the rat central nervous system is developmentally regulated. *Mol. Pathol.* **54,** 184–191 CrossRef Medline
72. Kyurkchiev, S., Yeger, H., Bleau, A. M., and Perbal, B. (2004) Potential cellular conformations of the CCN3(NOV) protein. *Cell Commun. Signal.* **2,** 9 CrossRef Medline
73. Heath, E., Tahri, D., Andermarcher, E., Schofield, P., Fleming, S., and Boulter, C. A. (2008) Abnormal skeletal and cardiac development, cardiomyopathy, muscle atrophy and cataracts in mice with a targeted disruption of the Nov (CCN3) gene. *BMC Dev. Biol.* **8,** 18 CrossRef Medline
74. Matsushita, Y., Sakamoto, K., Tamamura, Y., Shibata, Y., Minamizato, T., Kihara, T., Ito, M., Katsube, K., Hiraoka, S., Koseki, H., Harada, K., and Yamaguchi, A. (2013) CCN3 protein participates in bone regeneration as an inhibitory factor. *J. Biol. Chem.* **288,** 19973–19985 CrossRef Medline
75. Canalis, E., Smerdel-Ramoya, A., Durant, D., Economides, A. N., Beamer, W. G., and Zanotti, S. (2010) Nephroblastoma overexpressed (Nov) inactivation sensitizes osteoblasts to bone morphogenetic protein-2, but Nov is dispensable for skeletal homeostasis. *Endocrinology* **151,** 221–233 CrossRef Medline
76. Joliot, V., Martinerie, C., Dambrine, G., Plassiart, G., Brisac, M., Crochet, J., and Perbal, B. (1992) Proviral rearrangements and overexpression of a new cellular gene (nov) in myeloblastosis-associated virus type 1-induced nephroblastomas. *Mol. Cell. Biol.* **12,** 10–21 CrossRef Medline
77. Holbourn, K. P., Malfois, M., and Acharya, K. R. (2011) First structural glimpse of CCN3 and CCN5 multifunctional signaling regulators elucidated by small angle x-ray scattering. *J. Biol. Chem.* **286,** 22243–22249 CrossRef Medline
78. Brenner, M. C., Krzyzanski, W., Chou, J. Z., Signore, P. E., Fung, C. K., Guzman, D., Li, D., Zhang, W., Olsen, D. R., Nguyen, V. T., Koo, C. W., Sternlicht, M. D., and Lipson, K. E. (2016) FG-3019, a human monoclonal antibody recognizing connective tissue growth factor, is subject to target-mediated drug disposition. *Pharm. Res.* **33,** 1833–1849 CrossRef Medline
79. Gao, E., Lei, Y. H., Shang, X., Huang, Z. M., Zuo, L., Boucher, M., Fan, Q., Chuprun, J. K., Ma, X. L., and Koch, W. J. (2010) A novel and efficient model of coronary artery ligation and myocardial infarction in the mouse. *Circ. Res.* **107,** 1445–1453 CrossRef Medline
80. Galbán, S., Jeon, Y. H., Bowman, B. M., Stevenson, J., Sebolt, K. A., Sharkey, L. M., Lafferty, M., Hoff, B. A., Butler, B. L., Wigdal, S. S., Binkowski, B. F., Otto, P., Zimmerman, K., Vidugiris, G., Encell, L. P., *et al.* (2013) Imaging proteolytic activity in live cells and animal models. *PLoS One* **8,** e66248 CrossRef Medline

Connective tissue growth factor (CCN2) is a matricellular preproprotein controlled by proteolytic activation

Ole Jørgen Kaasbøll, Ashish K. Gadicherla, Jian-Hua Wang, Vivi Talstad Monsen, Else Marie Valbjørn Hagelin, Meng-Qiu Dong and Håvard Attramadal

J. Biol. Chem. 2018, 293:17953-17970.
doi: 10.1074/jbc.RA118.004559 originally published online September 27, 2018

Connective tissue growth factor (CCN2) is a matricellular preproprotein controlled by proteolytic activation

Kaasbøll OJ[1,2], Gadicherla AK[1,2 #], Wang JH[3], Monsen VT[1,2], Hagelin EMV[1,2], Dong MQ[3] and Attramadal H[1,2 *]

[1)] Institute for Surgical Research, Oslo University Hospital and University of Oslo, Oslo, Norway [2)] Center for Heart Failure Research, University of Oslo, Oslo, Norway [3)] National Institute of Biological Sciences, Beijing, China

---

Supporting information

Contains supplementary figures S1-S7 with figure legends, supplementary tables 1 and 2 and supplementary references.

Supplementary Figures

Fig. S1

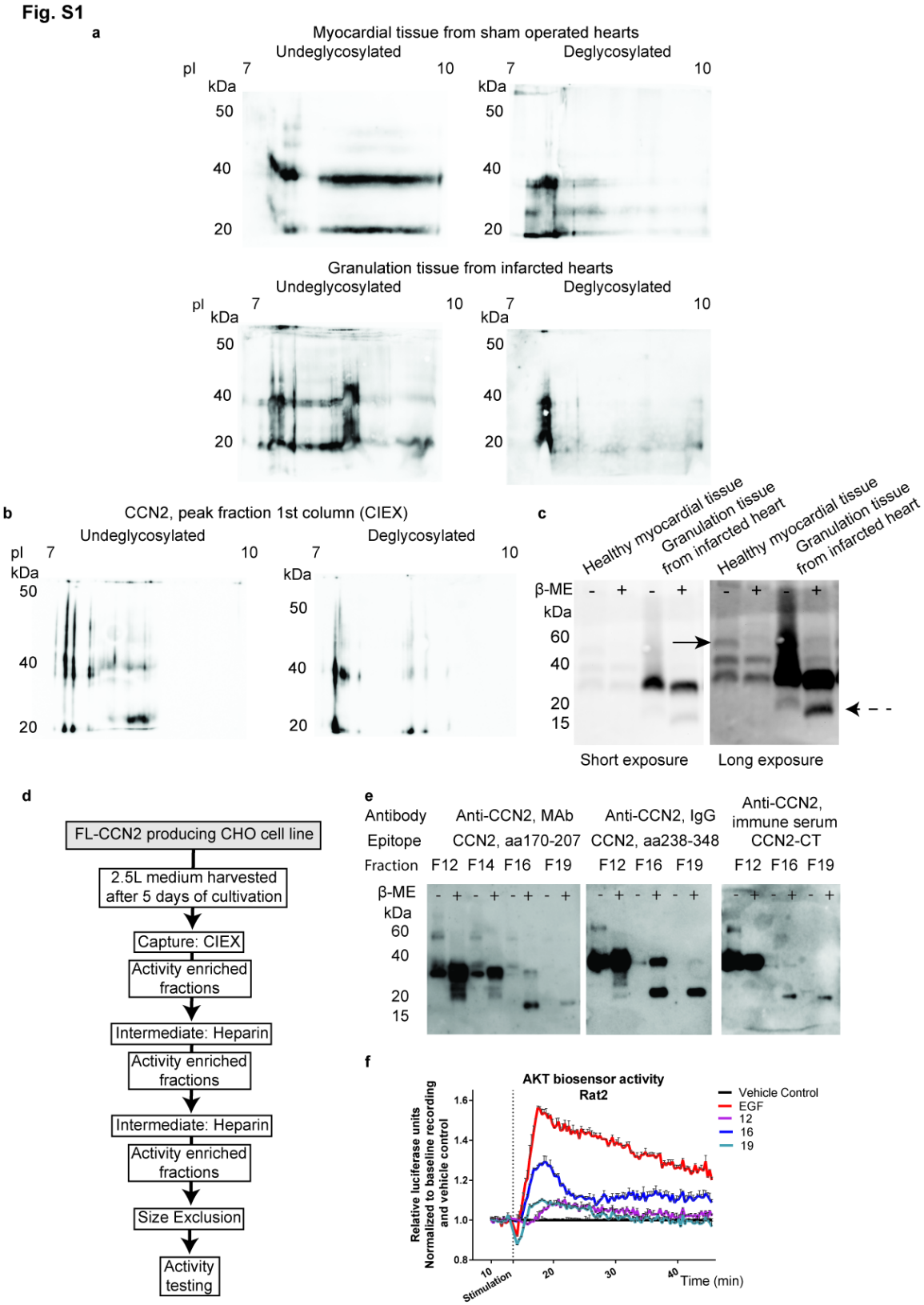

Supplementary Fig. S1. Glycosylation and degradation patterns of CCN2, and activity based purification of CCN2.

(**a**) Mice were subjected to experimental myocardial infarction or sham operation as previously reported(1). After 7 days, the heart was excised and myocardial tissue homogenates from 4 mice were

pooled, treated in the absence or presence of deglycosylating enzymes, and separated with 2D gel electrophoresis before immunoblotting with anti-CCN2 antibody (aa172-198 epitope). A representative blot of 2 independent experiments is shown. (**b**) The peak fraction eluted from the capture step of the FL-CCN2 purification was treated in the absence or presence of deglycosylation enzymes, subjected to 2D gel electrophoresis and immunoblotted with an anti-CCN2 antibody (aa172-198 epitope). A representative blot of 2 independent experiments is shown. (**c**) Extracts of healthy mouse myocardial tissue and granulation tissue from mouse hearts harvested 5 days after experimental myocardial infarction were separated by SDS-polyacrylamide gel electrophoresis under non-reducing or reducing conditions and subjected to Western blot analysis with an anti-CCN2 antibody (aa172-198 epitope). Arrow indicates a β-mercaptoethanol-sensitive immunoreactive band migrating at approximately 60 kDa under non-reducing conditions. Dashed arrow indicates the appearance of an immunoreactive band at migrating at approximately 18 kDa in the extract from cardiac granulation tissue under reducing conditions. (**d**) Chromatographic purification scheme for enrichment of fractions containing increasing amounts of phospho-AKT-stimulating activity. CIEX: cation exchange chromatography, Heparin: heparin affinity chromatography (**e**) Immunoblots of non-reduced and reduced fractions from the last step of the purification scheme shown in **d**. (**f**) phospho-AKT-stimulating activity in the fractions subjected to immunoblotting shown in **e** as assayed by the AKT phospho-kinase biosensor assay. Equal amounts of sample protein (μg protein) from the various fractions were assayed for AKT activity. The data presented in Panels e-f are representative of two independent chromatographic procedures. β-ME: β-mercaptoethanol.

Fig. S2

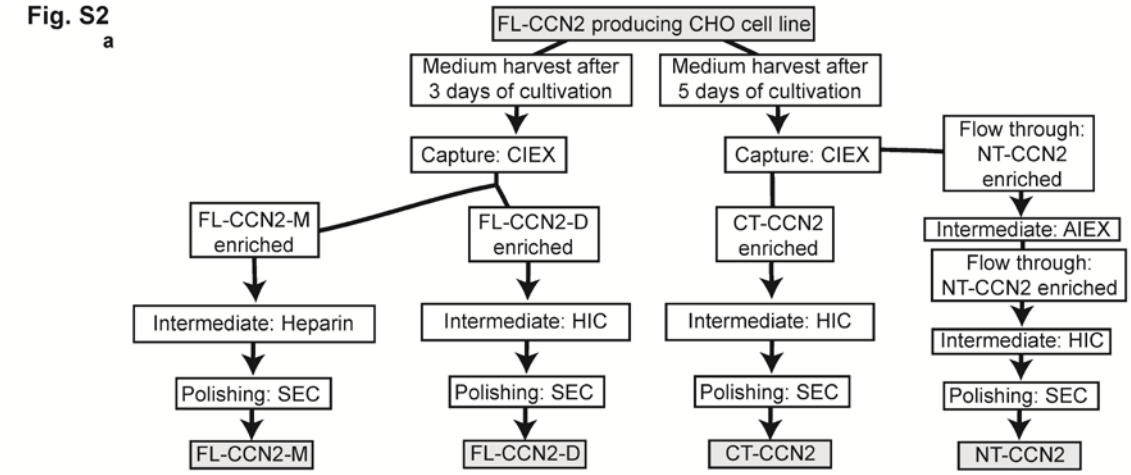

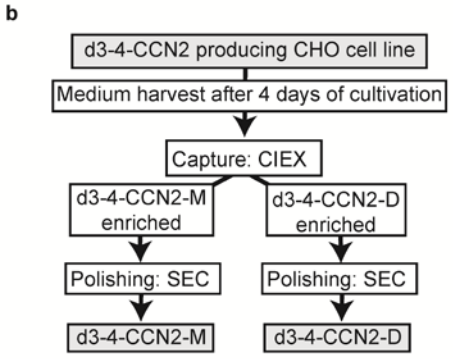

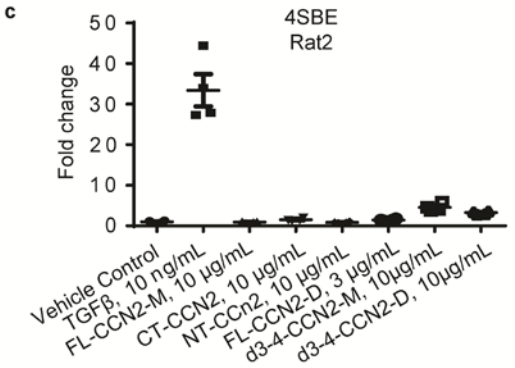

d FL-CCN2-D

```
  1 MTAASMGPVR VAFVVLLALC SRPAVGQNCS GPCRCPDEPA PRCPAGVSLV
 51 LDGCGCCRVC AKQLGELCTE RDPCDPHKGL FCDFGSPANR KIGVCTAKDG
101 APCIFGGTVY RSGESFQSSC KYQCTCLDGA VGCMPLCSMD VRLPSPDCPF
151 PRRVKLPGKC CEEWVCDEPK DQTVVGPALA AYRLEDTFGP DPTMIRANCL
201 VQTTEWSACS KTCGMGISTR VTNDNASCRL EKQSRLCMVR PCEADLEENI
251 KKGKKCIRTP KISKPIKFEL SGCTSMKTYR AKFCGVCTDG RCCTPHRTTT
301 LPVEFKCPDG EVMKKNMMFI KTCACHYNCP GDNDIFESLY YRKMYGDMA*
```

e NT-CCN2

```
  1 MTAASMGPVR VAFVVLLALC SRPAVGQNCS GPCRCPDEPA PRCPAGVSLV
 51 LDGCGCCRVC AKQLGELCTE RDPCDPHKGL FCDFGSPANR KIGVCTAKDG
101 APCIFGGTVY RSGESFQSSC KYQCTCLDGA VG CMPLCSMD VRLPSPDCPF
151 PRRVKLPGKC CEEWVCDEPK DQTVVGPALA AYRLEDTFGP DPTMIRANCL
201 VQTTEWSACS KTCGMGISTR VTNDNASCRL EKQSRLCMVR PCEADLEENI
251 KKGKKCIRTP KISKPIKFEL SGCTSMKTYR AKFCGVCTDG RCCTPHRTTT
301 LPVEFKCPDG EVMKKNMMFI KTCACHYNCP GDNDIFESLY YRKMYGDMA*
```

f CT-CCN2

```
  1 MTAASMGPVR VAFVVLLALC SRPAVGQNCS GPCRCPDEPA PRCPAGVSLV
 51 LDGCGCCRVC AKQLGELCTE RDPCDPHKGL FCDFGSPANR KIGVCTAKDG
101 APCIFGGTVY RSGESFQSSC KYQCTCLDGA VGCMPLCSMD VRLPSPDCPF
151 PRRVKLPGKC CEEWVCDEPK DQTVVGPALA AYRLEDTFGP DPTMIRANCL
201 VQTTEWSACS KTCGMGISTR VTNDNASCRL EKQSRLCMVR PCEADLEENI
251 KKGKKCIRTP KISKPIKFEL SGCTSMKTYR AKFCGVCTDG RCCTPHRTTT
301 LPVEFKCPDG EVMKKNMMFI KTCACHYNCP GDNDIFESLY YRKMYGDMA*
```

Amino acids identified by N-terminal Edman sequencing of CT-CCN2

AA	Step:	1	2	3	4	5	6	7	8	9	10	11	12	13	14	15	16	17	18	19	20
1.AA		A	Y	Y	L	E	D														
2.AA				T																	
3.AA				R																	
4.AA																					

g

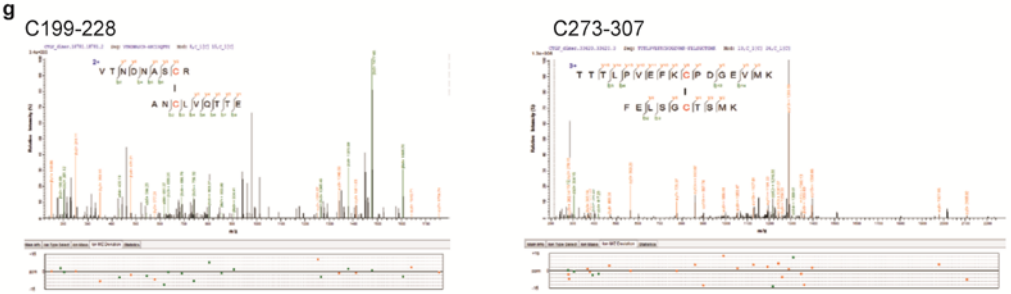

protein	best spectrum	Number of peptides supporting the identification results	Number of spectra supporting the identification results	best E-value	peptide
CCN2(273)-CCN2(307)	33620.33620.3.0.dta	20	1774	2,97E-15	TTTLPVEFKCPDGEVMK(10) FELSGCTSMK(6)
CCN2(199)-CCN2(228)	18781.18781.2.0.dta	3	66	4,03E-15	VTNDNASCR(8) ANCLVQTTE(3)

Supplementary Fig. S2. Purification scheme and characterization of various CCN2 entities
(**a**) Schematic of purification of various CCN2 entities from the DG44 CHO cell line expressing recombinant full-length human CCN2 (FL-CCN2). Cell culture medium from the stable DG44 CHO cell line expressing FL-CCN2 was harvested either 3 days or 5 days after subculture (in new cell

culture medium) for purification of FL-CCN2 monomer (FL-CCN2-M) and dimer (FL-CCN2-D), the major cleaved carboxyl-terminal fragment (CT-CCN2), and amino-terminal fragment of CCN2 (NT-CCN2) respectively. CIEX: cation exchange chromatography, HIC: hydrophobic interaction chromatography, Heparin: heparin affinity chromatography, SEC: Size Exclusion Chromatography, AIEX: anion exchange chromatography (**b**) As the mix of CCN2 entities in the conditioned medium from the stable CHO cell line secreting domain III-IV of CCN2 (d3-4-CCN2) was less complex, a simpler two-step purification scheme was sufficient for the purification of the monomeric (d3-4-CCN2-M) and dimeric (d3-4-CCN2-D) forms of d3-4-CCN2. (**c**) As TGFβ activity has been found to co-elute with full-length CCN2 in some chromatographic procedures (Lau, LF, personal communication), we tested the highly purified protein preparations used for activity assays to rule out contaminating TGFβ activity. Rat2 cells were adenovirally transduced with a SMAD-responsive luciferase reporter, serum-starved overnight, and stimulated with samples from the various protein preparations for 24 hours. (data points are technical replicates from 2 independent biological experiments). (**d**) Nano-LC-ESI-MS/MS analysis of the FL-CCN2-D separated by non-reducing SDS-PAGE demonstrating coverage of the entire secreted CCN2 peptide sequence (red lettering indicates detected peptides). (**e**) Nano-LC-ESI-MS/MS analysis of the NT-CCN2 fragment following separation by reducing SDS-PAGE demonstrating peptides from domain I (IGFBP domain) and domain II (vWC domain) only (red lettering indicates detected peptides). The complete lists of detected peptides from FL-CCN2-D and NT-CCN2 are shown in Supplemental Table 1. (**f**) The results of N-terminal sequence analysis (Edman degradation) of CT-CCN2 identifying the major cleavage site of secreted CCN2 (blue lettering showing detected amino acids). (**g**) MS spectra of identified disulfide-linked peptides in d3-4-CCN2-D utilizing the pLink-SS algorithm of the non-reduced sample. E-value < 0.0001 was required.

Fig. S3

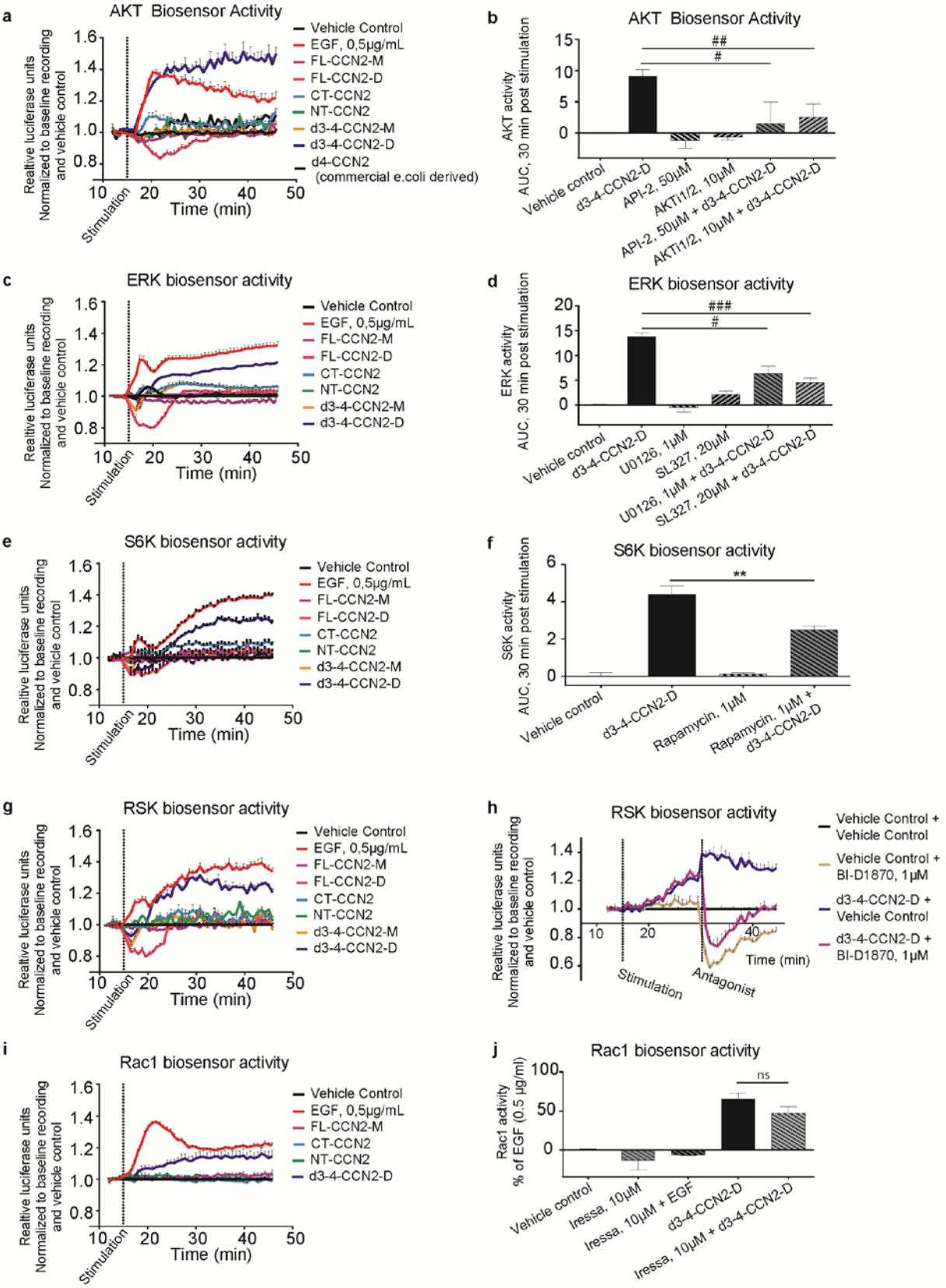

Supplementary Fig. S3. Time-course of biosensor assays and biosensor assay validation
Graphs depicting continuous recording of the relative luciferase units (RLU) in Rat2 cells stably transfected with one of the following biosensors; AKT/PKB (**a**), ERK1/2 (**c**), p70 S6 kinase (S6K) (**e**), p90 ribosomal S6 kinase (RSK) (**g**) and the GTPase Rac1 (**i**), serum-starved for 5-6h and stimulated

with 1 µg/mL of the indicated CCN2 protein preparations, or 0.5 µg/mL of EGF. As shown in the histograms, API-2 and AKTi1/2, selective inhibitors of AKT, efficiently prevented d3-4-CCN2-D-stimulated AKT-biosensor activity, whereas U0126 and SL126, selective inhibitors of MEK1/2, robustly reduced ERK biosensor activity (**b**, and **d)** validating the biosensor assays. The d3-4-CCN2-D-stimulated S6K biosensor activities were incompletely inhibited by rapamycin, indicating that the S6K biosensor partially reflects S6K activities. (**f**) For the RSK biosensor assay preincubation with pharmacological antagonists was not possible without large effects on the baseline signal, thus the RSK inhibitor BI-D1870 was added after 15min of d3-4-CCN2-D 2.5 µg/mL stimulation, demonstrating assay sensitivity to BI-D1870 (**h**). As there is, to our knowledge, no pharmacological inhibitor available of Rac1 GTP binding we investigated the sensitivities of EGF-stimulated and d3-4-CCN2-D-stimulated Rac1 biosensor activities to the EGF receptor kinase inhibitor gefitinib (Iressa). Gefitinib completely inhibited EGF-stimulated Rac1 biosensor activity, whereas d3-4-CCN2-D (2.5 µg/mL)-stimulated Rac1 activity was unaffected, indicating that EGF and CCN2 activate Rac1 via different receptor mechanisms (**j**). n≥2 independent experiments for all assays (**a-j**). The data in (**a, c, e, g, i, j**) were also used to generate the graphs in Figure 2. All error bars represent s.e.m. (**a-j**). Statistical significance of the differences between d3-4-CCN2-D uninhibited vs d3-4-CCN2 combined with indicated pharmacological inhibitors were calculated by 1-way ANOVA with Šidák's post hoc test in b and d, while two-tailed, unpaired t-test was utilized in f and j. $^{\#}P<0.01$; $^{\#\#}P<0.001$; $^{\#\#}P<0.0001$; ns: $P>0.05$; $^{**}P<0.01$.

Fig. S4

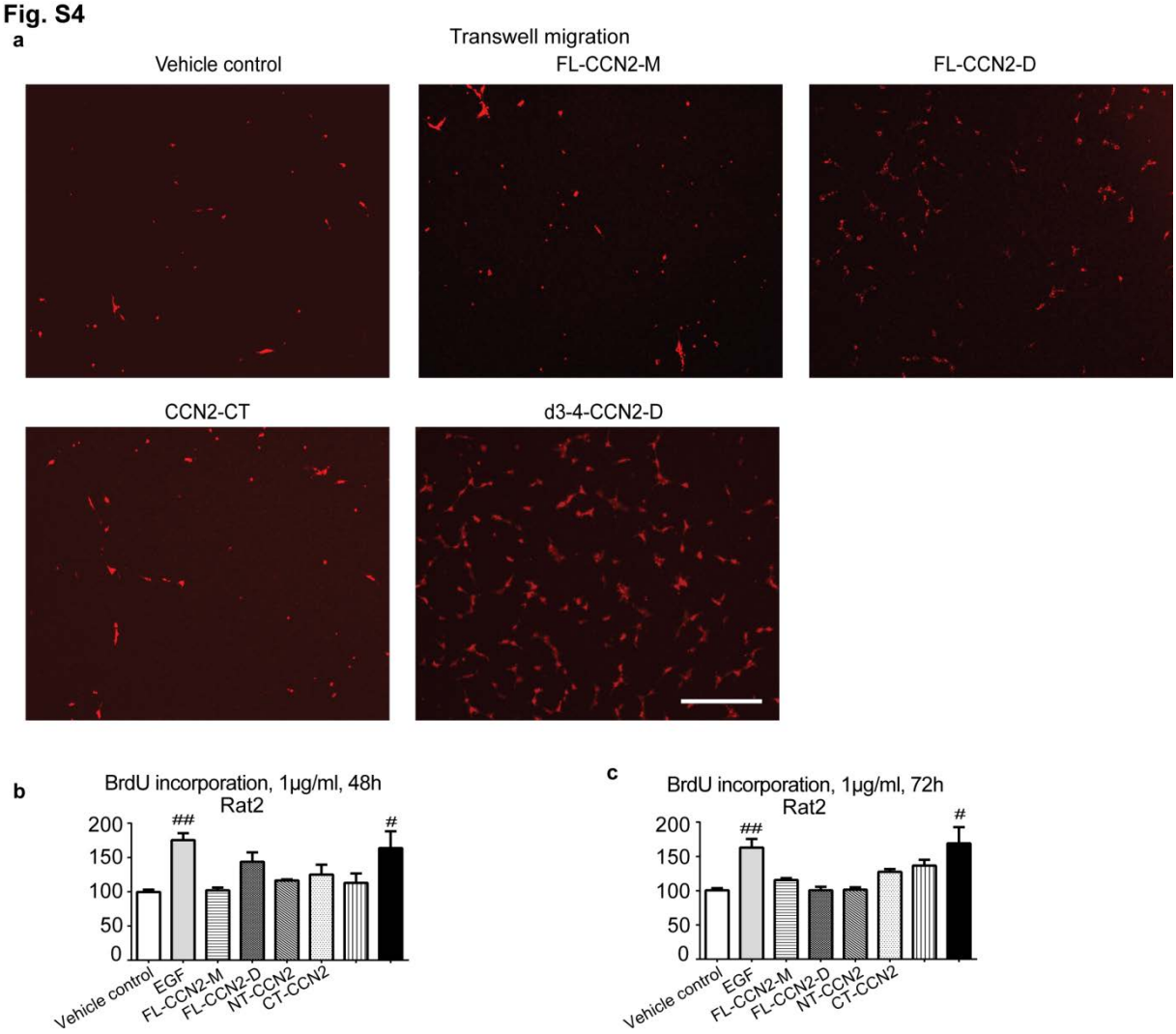

Supplementary Fig. S4. Cell physiological assays; representative photomicrographs and supporting assays

(a) Representative photomicrographs of transwell migration assays with Rat2 cells stimulated with indicated CCN2 entities. Scale bar is 50 µM. Quantification presented in Fig. 3b. (**b, c**) BrdU incorporation in serum-starved Rat2 cells stimulated with indicated CCN2 preparations for 48 hours (b) or 72 hours (c). n=2 biologically independent experiments. Statistical significance in **b** and **c** calculated by 1-way ANOVA with Šidák's post hoc test. $^{\#}P<0.01$ or $^{\#\#}P<0.0001$.

Fig. S5

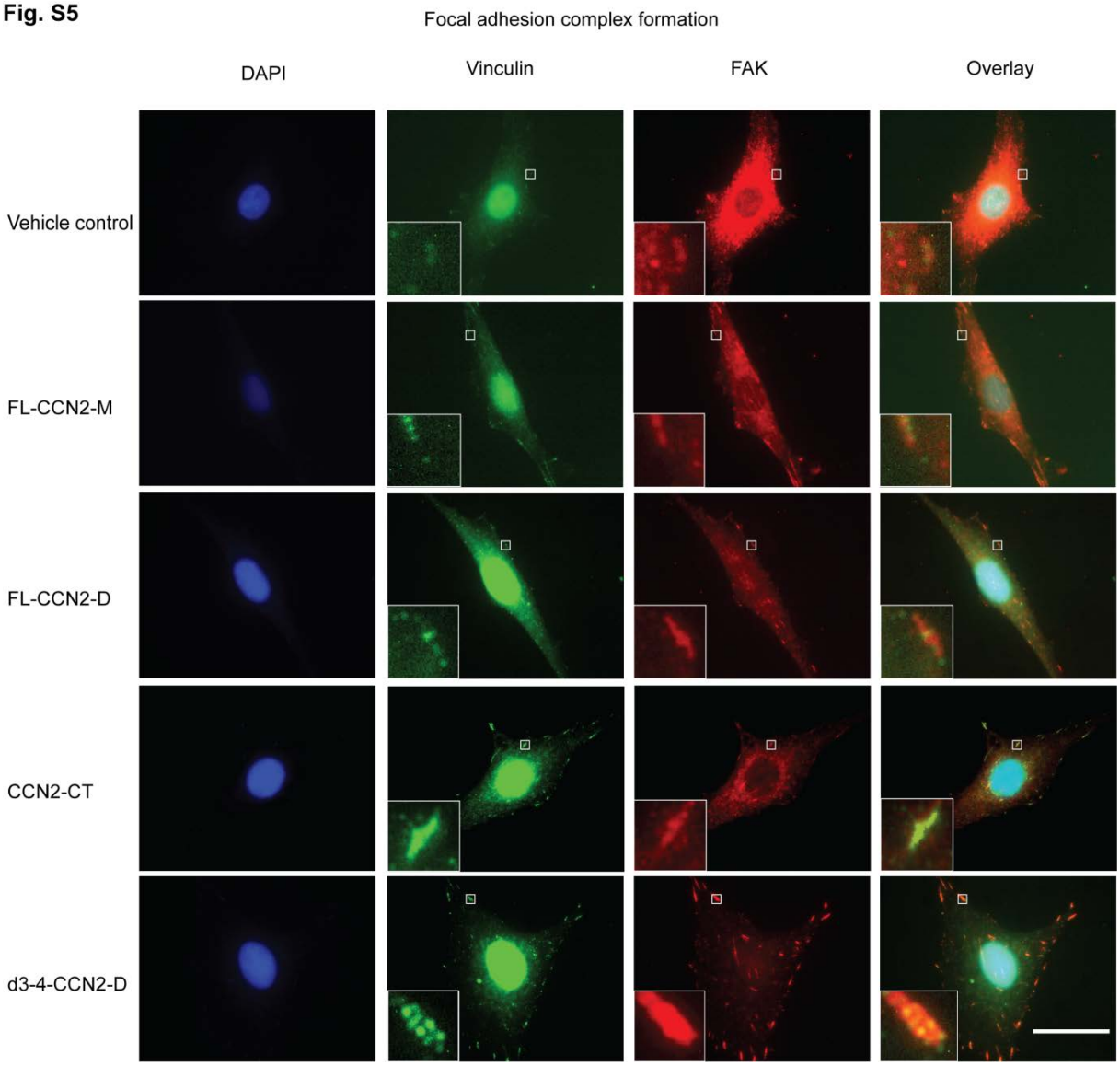

Supplementary Fig. S5. Cell physiological assays; representative photomicrographs
Representative photomicrographs of immunofluorescence staining of focal adhesion complexes (co-staining of Vinculin and FAK) in Rat2 cells stimulated with indicated CCN2 entities for 16 hours. Scale bar is 5 µM. Inserts are 8x magnifications of selected areas. Quantification presented in Fig. 3c in the main body of article.

Fig. S6

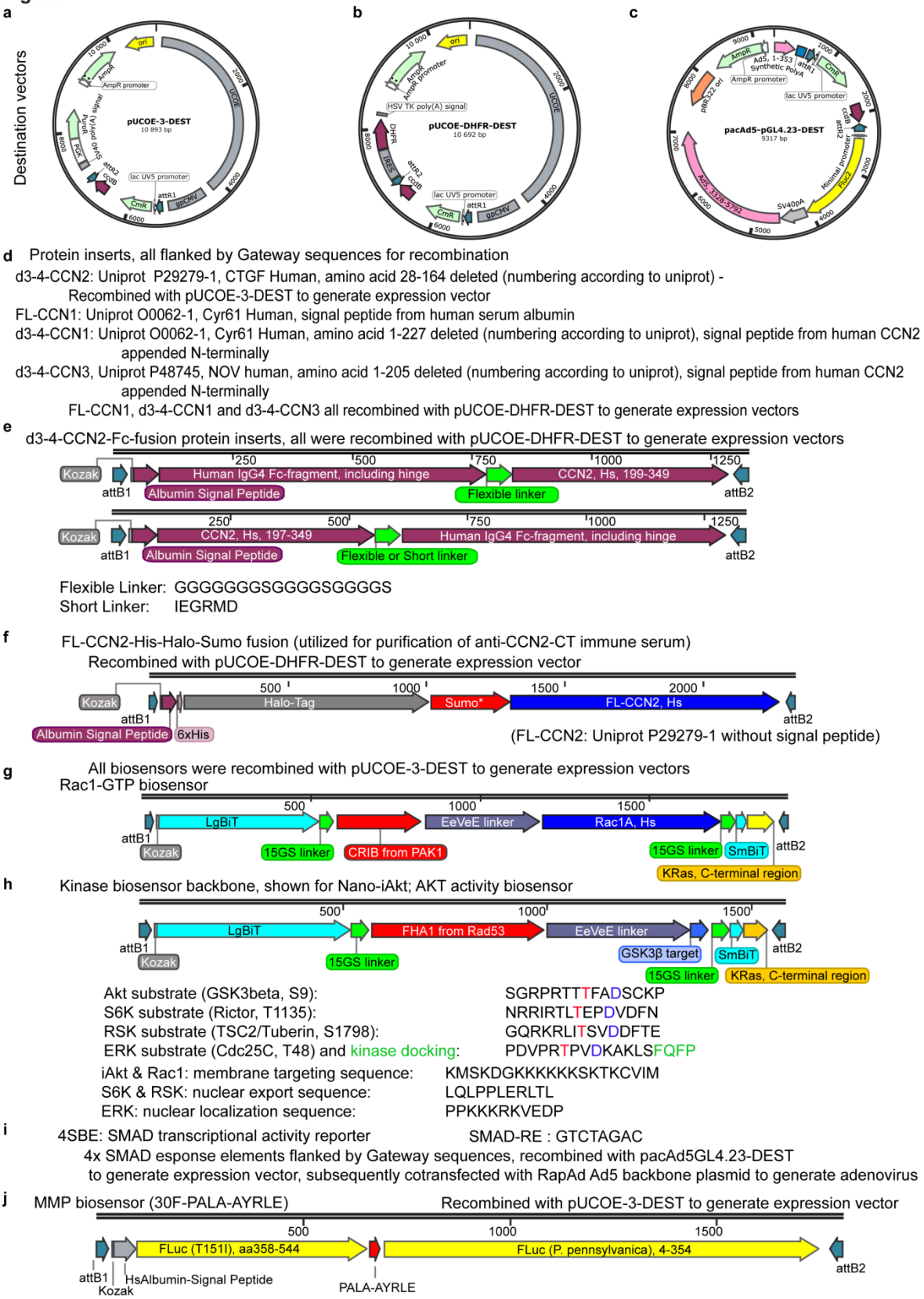

Supplementary Fig. S6. Schematics of generated plasmids

(**a**) The main features of the mammalian expression plasmid pUCOE-3-DEST is the Ubiquitous Chromatin Opening Element (UCOE) upstream of the promoter, a gateway cassette for insertion of gene-of-interest and the puromycin resistance (PuroR) gene for generation of stable cell lines. (**b**)

pUCOE-DHFR-DEST differs from pUCOE-3-DEST by having the puromycin resistance cassette replaced with an Internal Ribosomal Entry Site (IRES) and the cDNA encoding dihydrofolate reductase (DHFR) for generation and amplification of stable dihydrofolate reductase deficient ($DHFR^{-/-}$) DG44 CHO cell clones under selection with methotrexate. (**c**) pacAd5-pGL4.23-DEST is an adaptation of a shuttle vector (for generation of recombinant adenoviruses) with the insertion of a Gateway cassette upstream of a minimal promoter and open reading frame of firefly luciferase for efficient generation of recombinant adenovirus encoding a transcriptional reporter system. (**d-f**) Details on the protein sequences and orientation of fusion partners of inserts used to generate expression vectors for CHO cell expression of d3-4-CCN2, FL-CCN1, d3-4-CCN1, d3-4-CCN3, d3-4-CCN2-Fc-fusions and His-Halo-Sumo-FL-CCN2. (**g**) The split-NanoLuc luciferase (NanoBiT) adaptation of RaicuEV-Rac1(2) illustrating the N- and C-terminal fragments of NanoLuc luciferase (LgBiT and SmBiT, respectively) replacing YPet and SECFP in the original for generation of an enzyme complementation assay. (**h**) The NanoBiT adaptation of the AKT/PKB kinase sensor iAKT(3), again with the N- and C-terminal LgBiT and SmBiT replacing YPet and SECFP, respectively, and the list of kinase substrates and localization/targeting sequences used for generation of the biosensors of AKT, S6K, RSK and ERK kinase activities, as previously validated by Komatsu et al.(2). (**i**) The insert used to generate the adenovirus encoding a firefly luciferase transcriptional reporter of SMAD activity containing 4 SMAD-response elements (4SBE). (**j**) Schematic illustrating the adaptation of the GloSensor™ Caspase 3/7 to a secreted CCN2-^{177}PALAAYRLE^{185}-protease sensor.

Fig. S7

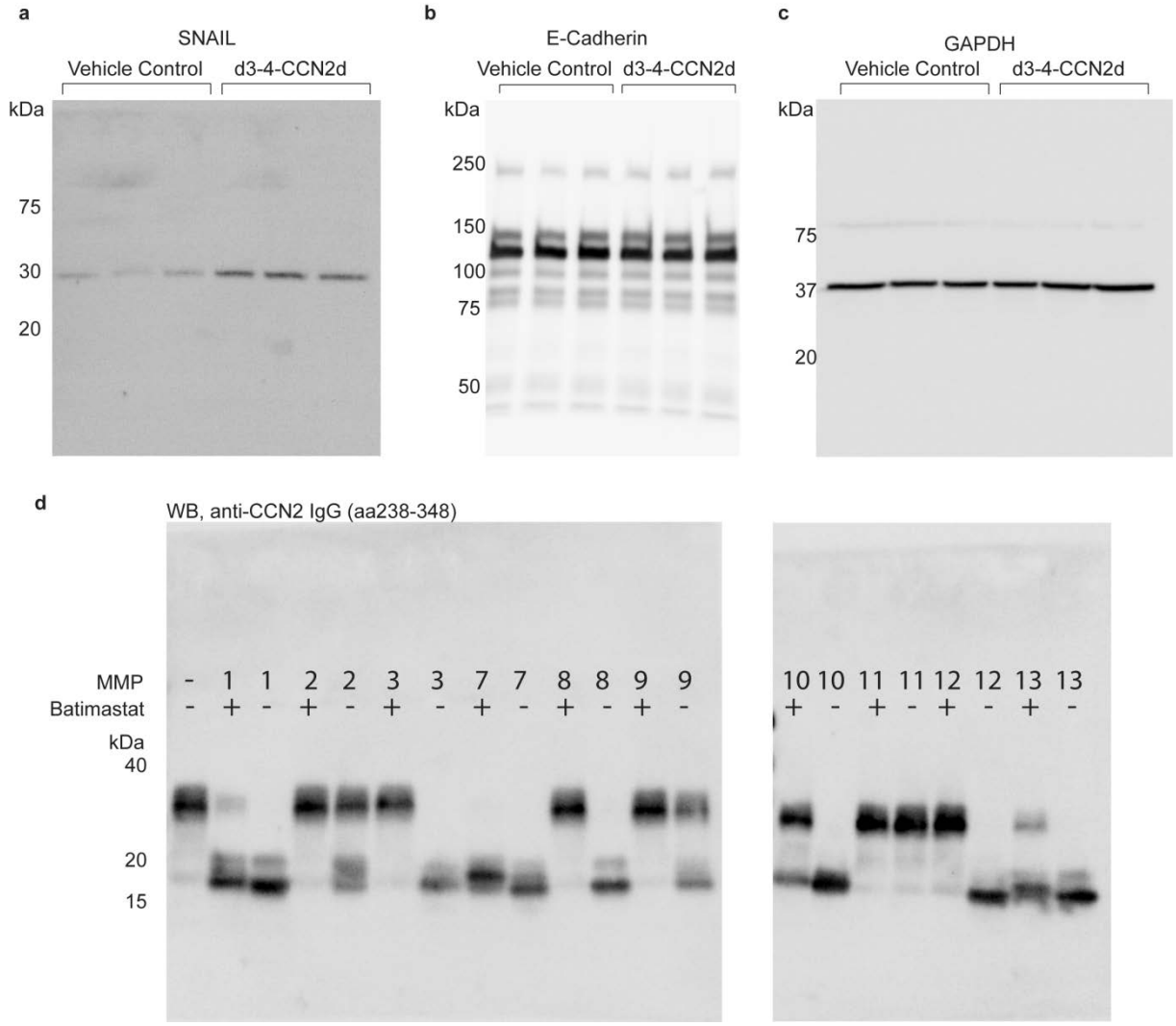

Supplementary Fig. S7. Uncropped blots
(**a-c**) Uncropped blots from Fig. 3f. (**d**) Uncropped blot from Fig. 4a.

Supplementary Table 1

FL-CCN2-D

	Num. of matches	Num. of sequences	emPAI	Coverage
connective tissue growth factor precursor [Homo sapiens]	188	25	23	70 %
keratin, type I cytoskeletal 10 [Homo sapiens]	38	17	1.4	
keratin, type II cytoskeletal 2 epidermal [Homo sapiens]	38	17	1.2	
keratin, type II cytoskeletal 1 [Homo sapiens]	36	15	1.0	
PREDICTED: connective tissue growth factor [Cricetulus griseus]	65	14	2.5	
keratin, type I cytoskeletal 9 [Homo sapiens]	8	5	0.3	
keratin, type II cytoskeletal 6B [Homo sapiens]	11	6	0.4	
SWISS-PROT:P02538 Tax_Id=9606 Gene_Symbol=KRT6A Keratin, type II cytoskeletal 6A	10	6	0.4	
SWISS-PROT:P00761|TRYP_PIG Trypsin - Sus scrofa (Pig).	48	5	2.3	
SWISS-PROT:P02769 (Bos taurus) Bovine serum albumin precursor	2	2	0.1	
serine protease HTRA1 precursor [Homo sapiens]	3	1	0.1	
ninein isoform 6 [Homo sapiens]	1	1	0.0	
trypsin-1 preproprotein [Homo sapiens]	2	1	0.1	
SWISS-PROT:P02662 Alpha-S1-casein - Bos taurus (Bovine).	1	1	0.1	

NT-CCN2

	Num. of matches	Num. of sequences	emPAI	emPAI (CCN2 aa 27-180)	Coverage	Coverage (CCN2 aa 27-180)
Keratin, type II cytoskeletal 1 [Homo sapiens]	64	20	1.72			
keratin, type I cytoskeletal 16 [Homo sapiens]	55	20	2.39			
keratin, type II cytoskeletal 6C [Homo sapiens]	47	16	1.22			
keratin, type II cytoskeletal 6C [Homo sapiens]	46	15	1.12			
keratin, type I cytoskeletal 10 [Homo sapiens]	42	15	1.26			
keratin, type I cytoskeletal 9 [Homo sapiens]	43	14	1.17			
connective tissue growth factor precursor [Homo sapiens]	89	15	2.53	3,87	41 %	93 %
keratin, type I cytoskeletal 14 [Homo sapiens]	35	11	1.0			
keratin, type II cytoskeletal 5 [Homo sapiens]	31	11	0.7			
keratin, type II cytoskeletal 2 epidermal [Homo sapiens]	27	11	0.66			
keratin, type I cytoskeletal 17 [Homo sapiens]	24	8	0.64			
Trypsin - Sus scrofa (Pig)	52	5	2.25			
keratin, type II cytoskeletal 4 [Homo sapiens]	6	3	0.17			
trypsin-1 preproprotein [Homo sapiens]	2	1	0.12			
hornerin [Homo sapiens]	2	1	0.01			
transmembrane channel-like protein 3 [Homo sapiens]	1	1	0.02			

Supplementary Table 2

Chromatography step	Column/media	Binding buffer	Elution buffer
CIEX (cation exchange)	HP SP Sepharose	150mM NaCl, 50mM MES, pH 6.0	2M NaCl, 50mM MES, pH 6.0
AIEX (anion exchange)	HP Q Sepharose	50mM NaCl, 60mM TrisHCl, pH 7.6	N/A
Heparin affinity	HP Heparin	150-300mM NaCl, 20mM Hepes, pH 7.0	2M NaCl, 20mM Hepes, pH 7.0
HIC (hydrophobic interaction chromatography)	SOURCE 15PHE 4.6/100 PE	1M $(NH_4)_2SO_4$, 0.5M NaCl, 20mM Hepes, pH 7.0	20mM Hepes, pH 7.0, 10% EtOH
SEC (size exclusion chromatography) (FL-CCN2-M, CT-CCN2)	HiLoad Superdex 16/600 75 pg	N/A	300mM NaCl, 20mM Hepes pH 7.0
SEC (size exclusion chromatography) (FL-CCN2-D, d3-4-CCN2-M, d3-4-CCN2-D, FL-CCN1-M, d3-4-CCN1-M, d3-4-CCN3-M and all d3-4-CCN2-Fc-fusions)	Superdex 200 Increase 10/300 GL	N/A	300mM NaCl, 20mM Hepes pH 7.0
Protein A capture (IgG and Fc-fragment)	HiTrap rProteinA FF	20mM NaH_2PO_4, pH 7.0	0.1M NaCitrate, pH 3.0
Antibody affinity purification	Halo-link Sepharose (Promega) coupled with FL-CCN2-His-Halo-Sumo	75mM TrisHCl, pH 8.0	0.1M Glycine HCl, pH 2.7, 0.5M NaCl

All chromatography media from GE Healthcare unless noted otherwise.

Supplementary References

1. Gao, E., Lei, Y. H., Shang, X., Huang, Z. M., Zuo, L., Boucher, M., Fan, Q., Chuprun, J. K., Ma, X. L., and Koch, W. J. (2010) A novel and efficient model of coronary artery ligation and myocardial infarction in the mouse. *Circ Res* **107**, 1445-1453
2. Komatsu, N., Aoki, K., Yamada, M., Yukinaga, H., Fujita, Y., Kamioka, Y., and Matsuda, M. (2011) Development of an optimized backbone of FRET biosensors for kinases and GTPases. *Mol Biol Cell* **22**, 4647-4656
3. Miura, H., Matsuda, M., and Aoki, K. (2014) Development of a FRET biosensor with high specificity for Akt. *Cell Struct Funct* **39**, 9-20